Received: 1 March 2023 | Revised: 22 June 2023 | Accepted: 4 July 2023

DOI: 10.1002/qj.4527

Quarterly Journal of the Royal Meteorological Society RMetS

RESEARCH ARTICLE

Evapotranspiration controls across spatial scales of heterogeneity

Mary Rose Mangan | **Oscar Hartogensis** | **Chiel van Heerwaarden** | **Jordi Vilà-Guerau de Arellano**

Meteorology and Air Quality Group, Wageningen University, Wageningen, The Netherlands

Correspondence
Mary Rose Mangan, Meteorology and Air Quality Group, Wageningen University, Wageningen, 6708 PB, The Netherlands.
Email: maryrose.mangan@wur.nl

Abstract

In semi-arid regions where irrigation causes thermal surface heterogeneities, evapotranspiration is controlled not only by the land surface but also by the interaction between the surface and the atmospheric boundary layer. The spatial scale of heterogeneity impacts the processes that drive the diurnal variability of evapotranspiration. In this study, we combine data with a conceptual, coupled land–atmosphere model to study the drivers of evapotranspiration across spatial scales of heterogeneity for the Land Interactions with the Atmosphere in the Iberian Semi-arid Environment (LIAISE) field campaign. We use a latent heat tendency equation as a diagnostic tool to quantify the contributions of various surface- and boundary-layer driven processes on surface latent heat flux. We define the following spatial scales based on surface characteristics: regional, landscape, and local. We find that, at the regional and landscape scales (>1 km), the feedback mechanisms between the surface fluxes and the resulting boundary-layer dynamics enhance the daily latent heat flux by 64% to 77%. Conversely, at the local scale (~100 m), surface-driven processes are most important for governing evapotranspiration. At the local scale, we find that the energy stored at the surface enhances evaporation in the late afternoon, which could explain the observed time lag between net radiation and latent heat flux. Furthermore, the combined effects of entrainment at the boundary-layer top and advection of heat and moisture enhance daily latent heat by 27% at the regional scale to 43% at the local scale. This analysis also has implications for the land-surface modelling community. It suggests that properly reproducing evapotranspiration to capture the relevant processes depends on capacity of the model to resolve the interaction of scales in surface heterogeneous conditions.

KEYWORDS

atmospheric boundary layer, evapotranspiration, land-surface models, surface heterogeneity

Abbreviations: ABL, atmospheric boundary layer; CLASS, Chemistry Land-surface Atmosphere soil Slab model; LIAISE, Land Interactions with the Atmosphere in the Iberian Semi-arid Environment; LSM, land-surface model.

1 | INTRODUCTION

In heterogeneous landscapes, evapotranspiration is driven not only by local surface processes, like radiation and turbulence intensity, but also by boundary-layer and mesoscale processes, like lateral advection of air and entrainment (Abdel-Aziz *et al.*, 1964; Rosenberg, 1969; Driedonks and Tennekes, 1984; Cuxart and Boone, 2020). The heterogeneity that results from locally applied irrigation in semi-arid areas can cause an increase in evapotranspiration in the irrigated fields through bidirectional land–atmosphere interactions. The coupling of the land–atmosphere interactions depends on the characteristic land-surface and spatial scale of heterogeneity (van Heerwaarden *et al.*, 2014). In this study, we aim to quantify the processes controlling evapotranspiration across spatial scales in the irrigated heterogeneous environment of the Land Interactions with the Atmosphere in the Iberian Semi-arid Environment (LIAISE) campaign in the summer of 2021 (Boone *et al.*, 2021; Mangan *et al.*, 2023). Specifically, our research questions are the following.

1 What are the processes that control evapotranspiration and its diurnal variability across spatial scales in a heterogeneous environment?
2 What is the relative importance of nonlocal controls on evapotranspiration in a heterogeneous area?
3 How do the contributions of evapotranspiration blend across spatial scales?

Land-surface models (LSMs) have difficulty reproducing the diurnal cycle of turbulent heat fluxes, particularly with the observed phase lag between net radiation and the turbulent heat fluxes (Renner *et al.*, 2021). Renner *et al.* (2021) suggest that one implication of LSMs not capturing the diurnal cycle of the surface fluxes correctly is a bias in the atmospheric boundary layer (ABL) dynamics, because the convective boundary layer is closely coupled to surface evaporative fluxes (Jacobs and Bruin, 1992; van Heerwaarden *et al.*, 2009). Because of the bidirectional interaction between the land surface and the ABL, boundary-layer dynamics could help to explain the diurnal cycle of surface fluxes. Coupled land–atmosphere models have been used to determine the sensitivity of evaporation to surface conditions (e.g., McNaughton and Spriggs, 1986; Wilson *et al.*, 1987; Ek and Holtslag, 2004) and the feedbacks between the land surface and the ABL (e.g., Jacobs *et al.*, 1992; Raupach, 2000; van Heerwaarden *et al.*, 2010). These studies focused either on evapotranspiration on a local scale where surface properties dominate, or evaporation on a regional scale where interactions between the ABL and the land surface become more important (McNaughton and Spriggs, 1986; Jacobs *et al.*, 1992). Because we are focused on the role of surface heterogeneity on the controls of evaporation, we must consider both regional and local-scale processes that govern land–atmosphere interactions.

Although there are studies describing the relevant processes that control surface fluxes in heterogeneous environments, including advection (Higgins *et al.*, 2013; Stoy *et al.*, 2013; Cuxart *et al.*, 2016), entrainment (McNaughton and Spriggs, 1986; van Heerwaarden *et al.*, 2009), thermal circulations (Patton *et al.*, 2005; Butterworth *et al.*, 2021), and organised boundary-layer turbulent structures (Kanda *et al.*, 2004; Inagaki *et al.*, 2006; Steinfeld *et al.*, 2007), how much each process contributes quantitatively to enhancing or reducing the surface latent heat flux remains uncertain. Over a realistic land surface, heterogeneities occur at a variety of spatial scales and we expect their influence to vary accordingly across them. These processes may communicate across spatial scales; therefore, it is important to determine the dominant processes that emerge across spatial scales.

To study the processes that control the diurnal cycle of evapotranspiration across spatial scales of heterogeneity, we employ the latent heat flux tendency equation introduced by van Heerwaarden *et al.* (2010; hereafter referred to as vH10) as a diagnostic tool to quantify the impact individual processes have on the total latent heat flux (LE). The LE tendency equation is a tool that allows us to attribute the evolution of LE to various local and nonlocal processes including radiation, advection, and entrainment processes. In vH10, the authors developed the framework and applied it to homogeneous regions: a grass site, the Cabauw tower in De Bilt, the Netherlands, and a desert site in Niamey, Niger. In this analysis, we expand the work of vH10 by applying the LE tendency equation to a heterogeneous area and, for the first time, we apply it using only observational data.

We describe the scale of heterogeneity for the LIAISE domain using the site-specific spatial scaling framework described by Mangan *et al.* (2023), where the scales of interest range from regional (~10 km) to landscape (~1 km) to a local field scale (~100 m). The spatial scales are characterised by surface thermal heterogeneity. The properties of the surface (e.g., soil moisture, crop cover, leaf-area index, etc.) are heterogeneous in space because of the irrigation patterns. The atmosphere feels the heterogeneity from the land surface through different flux regimes, which can be characterised by a Bowen ratio. Each scale is evaluated using both observations from the LIAISE campaign and a zeroth-order, mixed-layer model known as the Chemistry Land-surface Atmosphere Soil Slab model (CLASS: (Vilà-Guerau de Arellano *et al.*, 2015). We use the CLASS model to reduce the complexities of the study region and observational data to test the validity of

mixed-layer assumptions and the LE tendency equation in a realistic setting.

This analysis is structured as follows. In Section 2, we describe the research approach, which includes a data description and an introduction to the surface heterogeneity. In Section 3, we introduce the LE tendency equation from vH10 and describe how to apply it to observational data across the spatial scales. In Section 4, we show the results of the LE tendency equation analysis for both model and observational data. In Section 5, we discuss both the differences between drivers of evapotranspiration across spatial scales and the causes of the differences between the model and observational results. Furthermore, we compare the results of this analysis with those of vH10, where they used the LE tendency framework for two homogeneous surfaces: a well-watered grass field for the Cabauw tower and a desert site for Niamey.

2 | RESEARCH APPROACH

In this study, the LE tendency equation is the diagnostic tool; however, to apply it to a heterogeneous land surface, we first describe the data sources: the LIAISE field experiment and the CLASS model. Then we explain the research strategy applied to capture the heterogeneity by applying the spatial scaling scheme.

2.1 | Experimental and numerical data

The LIAISE experiment was designed to investigate the impact of human-induced surface heterogeneities on the spatio-temporal variability of surface fluxes and the development of ABL dynamics in a semi-arid region. It took place in the Ebro River Valley in the northeastern Iberian Peninsula (Figure 1) from July 15–30, 2021. The experiment consisted of measurements spanning from the leaf (e.g., observing the diurnal variability of stomatal conductance) to ABL scales (e.g., frequent radiosondes and aircraft measurements across the irrigated and dry areas). The LIAISE domain is characterised by thermal heterogeneity induced by irrigation. To the west of the domain, crops are irrigated annuals including maize and alfalfa (Figure 1). To the east side of the domain, crops are non-irrigated annuals, including winter cereal crops and non-irrigated perennial orchards. The daily evapotranspiration is up to 6 mm day^{-1} in the irrigated region, while the rain-fed fields have daily evapotranspiration rates of less than 1 mm day^{-1} during the campaign (Figure 1).

2.1.1 | The LIAISE campaign

During the LIAISE campaign, there were two "supersite" locations: an irrigated alfalfa field and a nonirrigated, fallowed winter-wheat field (Figure 1). At each site, there were 50-m meteorological towers, surface-energy budget stations, and hourly radiosondes launched. In addition to the supersites, there was a network of surface-energy budget stations in the dominant crop types in the LIAISE domain, including maize, a vineyard, and orchards, which were used to create surface and flux maps for the LIAISE domain shown in Figure 1. For more information about the LIAISE campaign and for an overview of available data, we refer to Boone *et al.* (2021) and Mangan *et al.* (2023). In this analysis, we examine a representative LIAISE composite day consisting of three days of full alfalfa cover (July 20–22, 2021) where the synoptic conditions and surface fluxes were similar to each other. We use this representative day to define the CLASS model experiment.

2.1.2 | The CLASS model

In this analysis, we used the coupled land–atmosphere model CLASS (Vilà-Guerau de Arellano *et al.*, 2015). CLASS is a zeroth-order mixed-layer model to replicate the composite, representative LIAISE day. Because it is a slab model, we define a representative land surface to represent each scale based on data collected during the LIAISE campaign. More information about capturing the spatial scales is given in the next section.

In the mixed-layer framework (Tennekes, 1973) shown in Figure 2, it is assumed that there is a surface layer where Monin–Obukhov similarity theory holds. Above the surface layer, there is a well-mixed ABL capped by a temperature inversion. The mixed-layer growth is driven by the surface buoyancy flux (Ball, 1960). Above the mixed layer, there is an entrainment zone separating the mixed layer from the free atmosphere. Soil moisture and temperature evolve using the force–restore method (Noilhan and Planton, 1989; Noilhan and Mahfouf, 1996; Vilà-Guerau de Arellano *et al.*, 2015), in which a reservoir of constant soil moisture and temperature in the root zone replenishes a top soil layer that interacts with the atmosphere. Surface fluxes are calculated using the Jarvis–Stewart land-surface model (Jarvis *et al.*, 1976; Stewart, 1988) and are coupled to the ABL dynamics. Turbulent transport between the surface and the atmosphere is controlled by the aerodynamic resistance (r_a) in the mixed layer. The implications of the choice of r_a will be discussed in Section 5.2.

2.2 | Spatial scaling of heterogeneity

In this study, we use the spatial scaling scheme from Mangan *et al.* (2023) to represent the spatial scales in the CLASS model. Within this framework, the regional scale

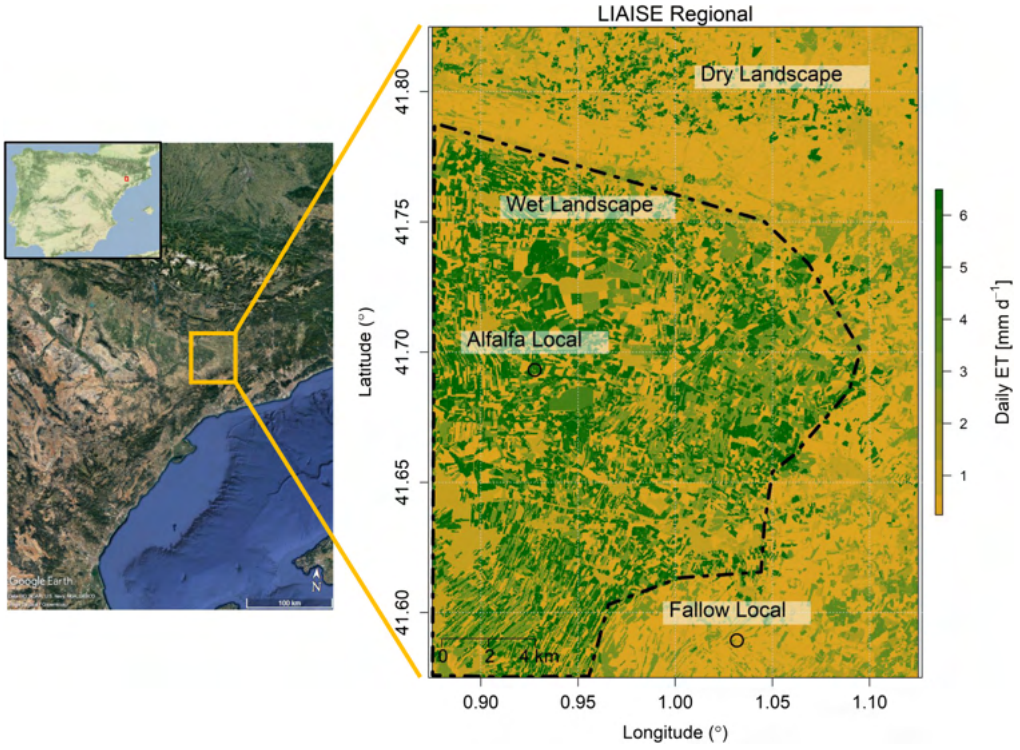

FIGURE 1 The LIAISE experiment took place in the Ebro River Valley in the northwest of the Iberian Peninsula (left). The land use in the LIAISE domain (right) is characterised by irrigated crops (west of the domain) and nonirrigated crops (east of the domain). The entire LIAISE regional scale is the ERA5 grid cell in the experimental region. [Colour figure can be viewed at wileyonlinelibrary.com]

(~10 km) matches the spatial extent of the ERA5 grid cell, and it encompasses both the irrigated and dry areas of the LIAISE domain (area represented in Figure 1). The regional scale consists of two landscape scales (~1 km) representing the wet and dry areas (dashed lines, Figure 1). At the landscape scale, heterogeneity arises from differences between fields. The local scale represents individual fields (~100 m) of either alfalfa or fallow local scales of surface properties (Figure 1). We represent each scale by changing surface properties (e.g., leaf-area index, soil moisture, and vegetative fraction) based on the observed, average values over each scale. In this study, we focus on the following scales: *LIAISE Regional*, *Wet Landscape*, and *Alfalfa Local*.

To represent these scales in the CLASS model, we change the land surface between scales to match a composite, parameter aggregate, view of the surface. The surface variables we modified included soil moisture, leaf-area index, and vegetative fraction, because the results were more sensitive to changing these properties than other surface properties including surface roughness and albedo. At the local scale, we include the advection of heat and moisture calculated from a network of automated weather stations, which show warm and dry-air advection for the alfalfa local scale during the afternoon. We refer to Section 4.2 and appendix B in Mangan *et al.* (2023) for a full description of the calculation of the advection term. For more details about representing these scales in the CLASS model, refer to table 1 in Mangan *et al.* (2023). For observations, we use the flux and surface maps described by Mangan *et al.* (2023) to represent the surface of the regional and landscape scales.

To quantify the emergence of differences between the scales, Figure 3 shows the surface-energy balance across the spatial scales in the LIAISE domain, with a focus on the irrigated region. The mean daily energy balance nonclosure varies from 35% at the alfalfa local scale to 10% at the wet landscape and regional scales. The net radiation (R_n) increases by 11% from the regional scale to the alfalfa scale. This is the negative effect. Because the surface temperature is higher at the regional scale, the outgoing longwave radiation is highest at the regional scale. The Bowen ratio decreases from a daily average of ~1.5 at the regional scale to ~0.01 at the alfalfa local scale. At the alfalfa local scale, H decreases to below zero in the afternoon. While the flux regimes differ across the spatial scales, the observed ABL is similar in both irrigated and nonirrigated areas. Mangan *et al.* (2023) found that the observed boundary layer can be replicated in the CLASS model using the composite surface fluxes from the LIAISE regional scale. This raises the question as to what processes are driving the increase of LE at the local scale compared with the regional and landscape scales.

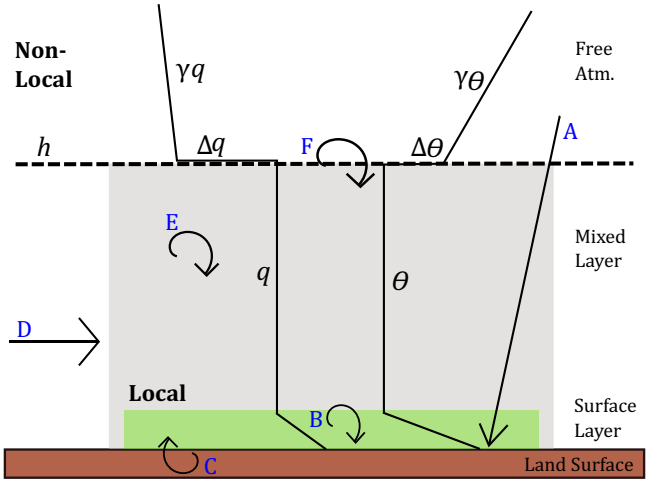

FIGURE 2 The coupled land–atmosphere view of the LE tendency equation (Equation 1). The surface layer is the lowest 10% of the mixed layer. The surface fluxes arise from the intersection between the surface layer and the land surface. Within the mixed layer, the potential temperature (θ) and the specific humidity (q) are constant with height. At the mixed-layer top (h), there are jumps in the state variables ($\Delta\theta$ and Δq). In the free atmosphere, the state variables have prescribed lapse rates ($\gamma\theta$ and γq). The terms of the LE tendency equation are indicated by arrows (the forcings) and the feedbacks (circles). The terms are labelled as follows: A, radiation forcing; B, surface-layer feedbacks; C, land-surface feedbacks; D, boundary-layer forcing; E and F, boundary-layer feedbacks. The boundary-layer feedbacks are split between the land-surface driven components (E) and the entrainment components (F). Local terms are defined as occurring within the one-dimensional column within the mixed-layer. The nonlocal terms are impacted by processes adjacent to the model column. [Colour figure can be viewed at wileyonlinelibrary.com]

3 | FUNDAMENTAL ANALYSIS CONCEPTS

In this section, we start by introducing the LE tendency equation. For our purposes, we split the terms into surface- and boundary-layer-driven processes. We conclude this section by describing the preparation to apply the LE tendency equation to observational data.

3.1 | Latent heat tendency equation

The LE tendency equation, introduced by vH10, is used to determine the controls—both surface and boundary-layer driven—on LE. The equation is obtained by taking the time derivative of the Penman–Monteith potential evapotranspiration equation, then substituting mixed-layer equations (Tennekes, 1973) into the tendencies of temperature and humidity. We refer to the appendix in van Heerwaarden *et al.* (2010) for the complete derivation. In this way, they were able to create a framework for determining the drivers of evapotranspiration in a mixed-layer environment (Figure 2).

The LE tendency equation is composed of five terms, which are named the same as vH10. The terms titled *forcing* represent external inputs of energy, temperature, or moisture into the system that impact evapotranspiration. The terms titled *feedback* represent processes that both influence and are influenced by surface evaporation. In this analysis, we separate the terms into two groups: surface processes and boundary-layer processes as shown by Figure 2. Equation 1 is the tendency of LE as a function of the forcing and feedback terms (vH10), in which the variables are defined in Table 1. In Equation 1, Figure 2, and Table 1, we introduce terms A–F to represent the different

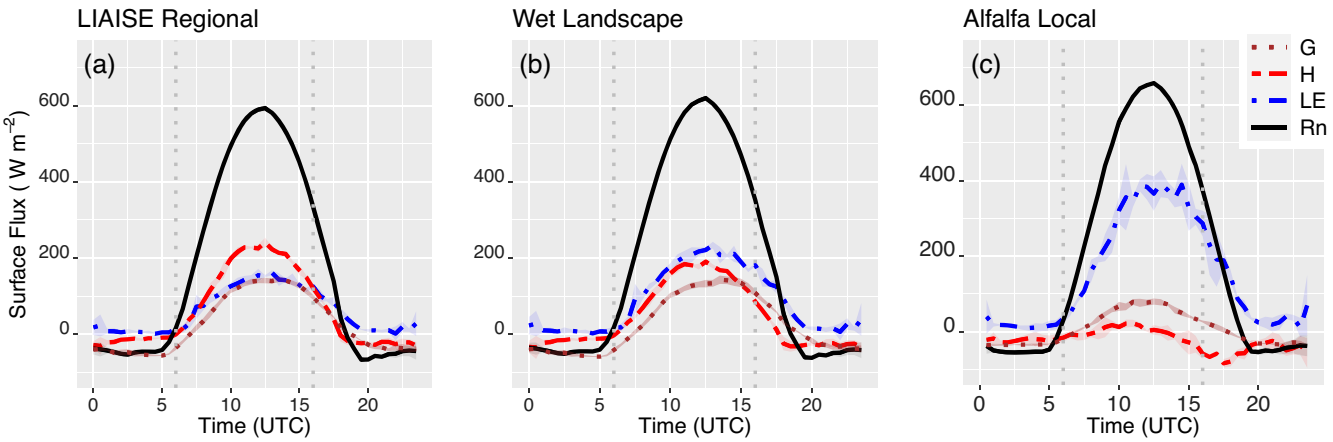

FIGURE 3 The observed diurnal cycle of sensible and latent heat flux for the LIAISE domain at the LIAISE regional scale, the Wet Landscape scale, and the Alfalfa Local scale. [Colour figure can be viewed at wileyonlinelibrary.com]

TABLE 1 The variables in the LE tendency Equation 1.

Variable	Variable name	Units	Terms
q_{sat}	Mixed-layer saturated specific humidity	kg kg^{-1}	A, B, C, D, E
T	Mixed-layer temperature	K	A, B, C, D, E
α	Surface albedo	–	A
S_{in}	Incoming shortwave radiation	W m^{-2}	A
L_{in}	Incoming longwave radiation	W m^{-2}	A
q	Mixed-layer specific humidity	kg kg^{-1}	B
LE	Latent heat flux	W m^{-2}	B, C, E
r_s	Surface resistance	s m^{-1}	A, B, C, D, E
r_a	Aerodynamic resistance	s m^{-1}	A, B, C, D, E
L_{out}	Outgoing longwave radiation	W m^{-2}	C
G	Ground heat flux	W m^{-2}	C
H	Sensible heat flux	W m^{-2}	D, E
adv_θ	Advection of potential temperature	K s^{-1}	D
adv_q	Advection of specific humidity	kg kg^{-1} s^{-1}	D
h	Mixed-layer height	m	E
w_e	Entrainment velocity	m s^{-1}	E
$\Delta\theta$	Entrainment jump in potential temperature	K m^{-1}	E
Δq	Entrainment jump in specific humidity	kg kg^{-1} m^{-1}	E

Note: The final column "Terms" lists the terms of the LE tendency equation in which a variable is found.

drivers of LE. Each term contains dq_{sat}/dT (the change in saturated specific humidity with temperature), which is calculated using the Clausius–Clapeyron equation. Constants in Equation 1 include the density of air (ρ), latent heat of vaporisation (L_v), and the heat capacity of air at a constant pressure (c_p). The physical interpretation of each of these drivers of LE follows in the next sections.

$$\frac{dLE}{dt} =$$

$c_0 \frac{dq_{sat}}{dT}\left\{(1-\alpha)\frac{dS_{in}}{dt} + \frac{dL_{in}}{dt}\right\}$	A. Surface Radition	Forcing	Local
$-c_0\left(\frac{\rho c_p}{r_a^2}(q_{sat} - q) - LE\frac{c_p}{L_v}\frac{r_s}{r_a^2}\right)\frac{dr_a}{dt}$	B. Surface-layer	Feedback	Local
$-c_0\frac{dq_{sat}}{dT}\frac{dL_{out}}{dt} - c_0\frac{dq_{sat}}{dT}\frac{dG}{dt} - c_0 LE\frac{c_p}{L_v}\frac{1}{r_a}\frac{dr_s}{dt}$	C. Land Surface	Feedback	Local
$+c_0\left(H\frac{d^2q_{sat}}{dT^2} + \frac{\rho c_p}{r_a}\frac{dq_{sat}}{dT}\right)\{adv_\theta\} - c_0\frac{\rho c_p}{r_a}\{\text{adv}_q\}$	D. Boundary-layer	Forcing	Nonlocal
$+ c_0\left(H\frac{d^2q_{sat}}{dT^2} + \frac{\rho c_p}{r_a}\frac{dq_{sat}}{dT}\right)\left\{\frac{w_e\Delta\theta}{h}\right\} - c_0\frac{\rho c_p}{r_a}\left\{\frac{w_e\Delta q}{h}\right\}$	E. Boundary-layer	Feedback	Nonlocal
$+ c_0\left(H\frac{d^2q_{sat}}{dT^2} + \frac{\rho c_p}{r_a}\frac{dq_{sat}}{dT}\right)\left\{\frac{H}{\rho c_p h}\right\} - c_0\frac{\rho c_p}{r_a}\left\{\frac{LE}{\rho L_v h}\right\}$	E. Boundary-layer	Feedback	Local

where

$$c_0 = 1/\left[\frac{dq_{\mathrm{sat}}}{dT} + \frac{c_{\mathrm{p}}}{L_{\mathrm{v}}}\left(1 + \frac{r_{\mathrm{s}}}{r_{\mathrm{a}}}\right)\right]. \quad (2)$$

3.1.1 | Surface processes

The surface processes that influence LE are driven either by the land surface or by the surface layer of the atmosphere. The surface processes include radiation forcing, surface-layer feedbacks, and land-surface feedbacks. These processes are responsible for partitioning the available energy at the surface.

Surface radiation forcing (A)

The surface radiation forcing represents the total radiative energy introduced to the system (Figure 2, Arrow A). The individual contributions to this term are the total shortwave radiation and the incoming longwave radiation at the surface. Although radiation originates outside the ABL, this term is considered a "surface process" because it acts at the surface. For example, with an increase of shortwave radiation in the middle of the day, there is more energy available to increase LE. Likewise, an increase in incoming longwave radiation, for example because of low clouds, can also increase LE.

Surface-layer feedbacks (B)

The surface layer is approximated as the lowest 10% of the ABL in our mixed-layer framework (Vilà-Guerau de Arellano *et al.*, 2015). The surface-layer feedback describes the processes that govern r_{a}, which represents the atmospheric mixing to connect the surface with the atmosphere (Figure 2, Arrow B). Consider, for example, a case of negative sensible heat flux in the afternoon when LE was high, as was observed in LIAISE (Figure 3). Sensible heat flux (H) was negative in the afternoon when LE was high. If H is negative, then the surface layer is statically stable, which increases r_{a}, which in turn decreases LE. This case has a negative surface-layer feedback.

Land-surface feedbacks (C)

The land-surface feedbacks control the partitioning of available energy at the surface (Figure 2, Arrow C) through the surface temperature. The term can be divided into three parts: L_{out}, ground heat flux (G), and r_{s}. These terms assign the incoming energy into heating of the surface, conduction into the ground, and the partitioning of available energy into H and LE, respectively. The effect of soil drying on LE is applied indirectly through the r_{s} effect. In the case of the CLASS model—unlike observations—there is a constant source of soil moisture at the rooting depth, so one would expect the r_{s} term to be influenced more by the surface-layer vapour-pressure deficit than by soil drying.

3.1.2 | Boundary-layer processes

Unlike the surface processes, the boundary-layer processes control the surface energy partitioning indirectly by altering either the temperature or moisture of the ABL. These processes change the vapour-pressure deficit between the atmosphere and the surface, which can enhance or reduce LE. The boundary-layer processes are split into forcing terms (e.g., advection of heat and moisture) and feedback terms (e.g., surface and entrainment warming and drying).

Boundary-layer forcing (D)

The boundary-layer forcing term represents advection of temperature and moisture into the column (Figure 2, Arrow D). The method does not consider the origins of the advection; physically, advection could arise from mesoscale thermal circulations, synoptic pressure gradients, or locally from adjacent fields. Therefore, we interpret this term as a large-scale forcing. We combine all the potential causes of advection to test the sensitivity of LE to the inclusion of temperature or moisture advection. This is considered a nonlocal process.

Boundary-layer feedbacks (E and F)

The boundary-layer feedbacks are separated into four terms: surface warming, surface moistening, entrainment warming, and entrainment drying (Figure 2). The surface terms are local because they arise from processes within the slab model (Arrow E), while the entrainment terms are nonlocal because they are influenced by synoptic forcing from the free atmosphere (Arrow F). To understand the role of boundary-layer feedbacks, again consider the alfalfa local case where H becomes negative in the afternoon. This increases the specific humidity and decreases the atmospheric temperature, both of which would reduce the vapour-pressure deficit, so both surface warming and surface moistening feeds back into decreasing LE.

3.2 | Observational data preparation

The LE tendency equation was designed to be used with output from the CLASS model. To calculate the terms directly from observations from the LIAISE campaign, we made a number of assumptions for data preparation. In general, there were two steps of data preparation necessary before evaluating the LE tendency equation from observations: (1) upscale field-scale observations to represent the regional and landscape scales, and (2) fit a

polynomial function to the data so that time derivatives are smooth. In the subsequent paragraphs, we briefly introduce the corrections. More details can be found in Appendix A.

In order to represent different spatial scales of observations, we used the surface and flux maps described by Mangan *et al.* (2023). Using these maps, we calculate the radiation and surface-energy budgets for each spatial scale. We force surface-energy budget closure by redistributing the excess energy to H and LE by preserving the observed Bowen ratio (Twine *et al.*, 2000) to be consistent for application in the LE tendency equation. For the boundary-layer characteristics, we used the average mixed-layer values of the radiosondes launched from the wet and dry areas to approximate the regional scale, because the observed mixed layer is similar between the two sites. For the landscape and local scales, we used the radiosondes launched within that landscape alone. As will be discussed later, there are several variables calculated directly in the CLASS model that do not match with observed quantities, including aerodynamic resistance and surface temperature. In these cases, we calculated the terms using the same formulation as the CLASS model (Appendix A). We use the mixed-layer wind observed by the radiosondes to calculate the mixed-layer atmospheric resistance.

Because observational data are noisier than model data, taking the derivative of observational data introduces errors in the calculation of the LE tendency equation. We selected the lowest-order polynomial fit that captured the dynamic cycle of the data. For most variables, this was a fourth-order polynomial fit. In this way, we could eliminate some of the noise from the observational data, and we could increase the temporal resolution of the data from 30 to 1 min, which lead to better results when applying the tendency equation. Using observational data allows us to test the efficacy of the equation in an environment where the mixed-layer assumptions fail.

4 | RESULTS

In this section, results from the LE tendency equation are displayed for both the CLASS model and the observations at the LIAISE regional, wet landscape, and alfalfa local scales. Note that, while we refer to the scales as regional, landscape, and local, this refers to the site-specific LIAISE regional, wet, and alfalfa scales—the relevant scales of surface-driven heterogeneity in this experiment. These scales of heterogeneity are nested and may interact with each other simultaneously. We start by showing the total tendency of LE (left-hand side of Equation 1), and then we narrow the focus to specific surface- and boundary-layer processes. Although we display results for both the observations and the CLASS model, we focus on the results from the CLASS model for process understanding. By using the CLASS model, unlike when we appy the LE tendency equation to observations, the LE tendency equation closes when it is applied to the results of the CLASS model. After discussing the relevant processes in Section 5.1, we confront the model with data in the discussion in Section 5.2.

4.1 | Total tendency

The total tendency of LE is shown in Figure 4. The lines show the CLASS model, runs while the points depict the observations. The leftmost panel is the result for the LIAISE regional scale, the middle panel is for the wet landscape scale, and the right panel is for the alfalfa local scale. At all scales, the model matches the observed total LE tendency well. Additionally, the peak LE tendency, which relates to the inflection point in the morning LE, occurs at all scales at approximately 0900 UTC; however, the peak is highest at the local scale. At all scales, the zero-crossing in the tendency occurs just after solar noon (at 1230 UTC at all scales).

To analyse which terms contribute to LE, one can also integrate the daily tendency to show each component's relative contribution to the daily LE. The terms are normalised with the total daily LE such that each scale sums to one. In Figure 5, we display the daily relative contribution of each term of the LE tendency equation across spatial scales. The results of the CLASS modelling scheme are in the top panel of Figure 5, while the results of the observations are in the bottom panel. Generally, the sign and pattern of the relative contributions to LE tendency match between the observations and the model, except for the surface-layer feedbacks. This indicates that the mixed-layer LE tendency framework holds reasonably well using observations that violate mixed-layer theory. The differences in magnitude of the components of the LE tendency equation will be discussed in more detail in the subsequent sections of this study.

According to Figure 5, radiation forcing generally enhances LE and its impact increases at smaller spatial scales. The land-surface feedbacks reduce LE at all scales, and its relative effect is strongest at the regional scale. According to the CLASS model, the surface-layer feedback decreases the LE at the regional and landscape scales, while it slightly enhances LE at the local scale. The boundary-layer forcing term increases LE at all scales, but its effect is strongest at the local scale, where the prescribed advection is the strongest. Finally, the boundary-layer feedbacks enhance LE at all scales, but the relative impact decreases towards smaller spatial scales,

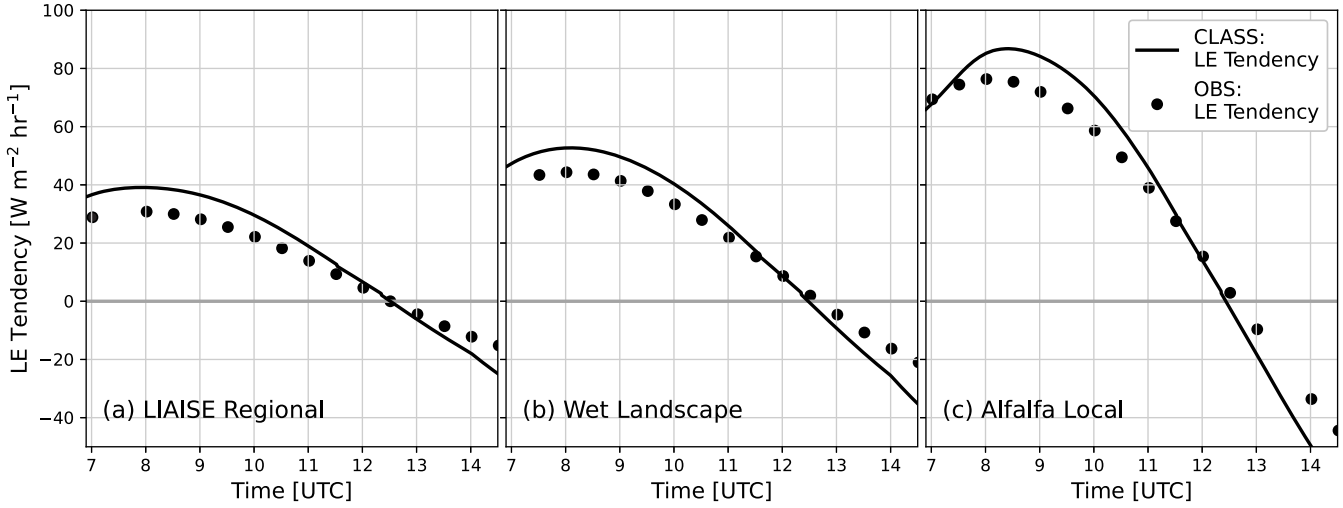

FIGURE 4 The tendency of latent heat over the LIAISE aggregate day for (a) the LIAISE regional scale, (b) the Wet Landscape scale, and (c) the Alfalfa Local scale. The observations are shown by the dots and the results from the CLASS model are shown by the lines.

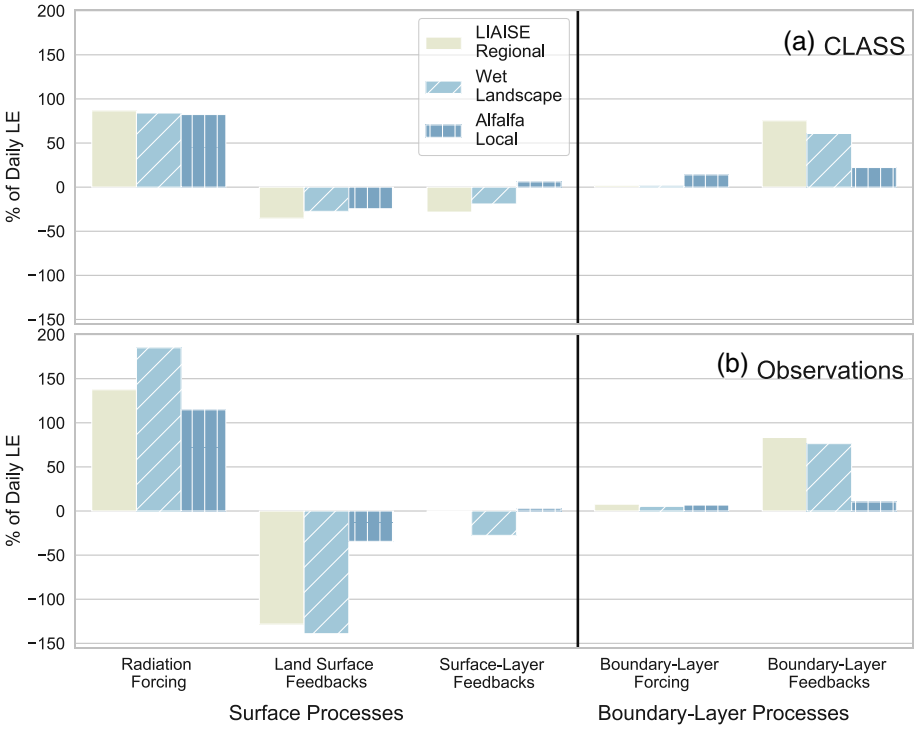

FIGURE 5 Relative contribution of each term of the LE tendency equation for (a) the CLASS model and (b) the observations. The hue and hatching denote the spatial scale. [Colour figure can be viewed at wileyonlinelibrary.com]

although the absolute contributions are highest at the local scale.

4.2 | Surface processes

Radiation forcing

The radiation forcing term consists of two components: the net shortwave and the downwelling longwave radiation. Together, these terms represent the total energy available at the surface. Figure 6 shows the components of the radiation term over 1 day at the three scales. The points represent observations and the lines represent the model results.

The radiation appears to drive the total tendency signal (Figure 6). The peaks in these signals occur in the middle of the morning, when radiation is increasing the most. Before noon, radiation enhances LE, and after noon, it reduces LE. The radiation term is mainly controlled by the net shortwave radiation component. The radiation component accounts for approximately 80% of the total LE in

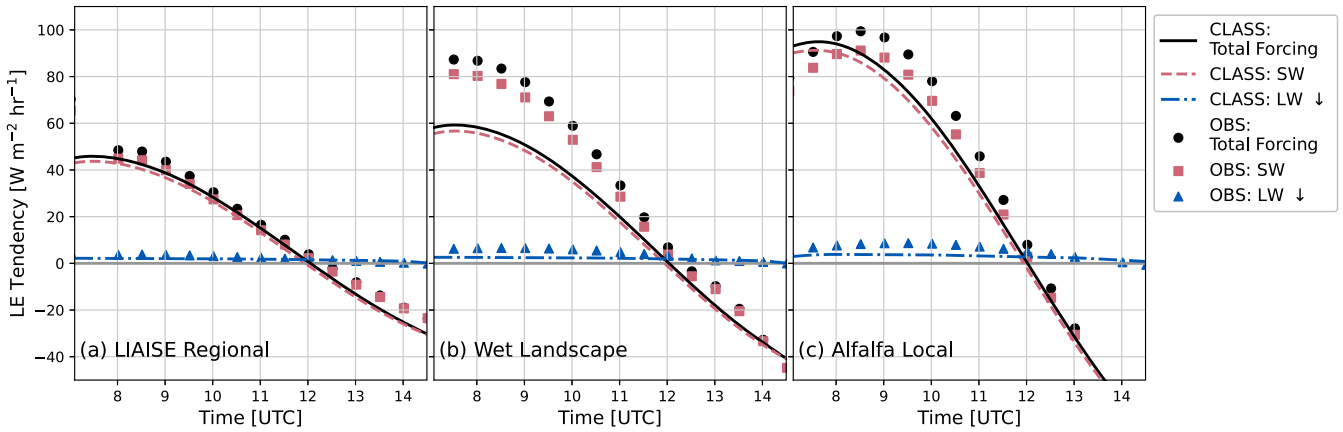

FIGURE 6 The radiation forcing term from the latent heat tendency equation for (a) the LIAISE regional scale, (b) the Wet Landscape scale, and (c) the Alfalfa Local scale. The lines are model results and the points are from the observations. The solid lines and circles are the total radiation forcing. The shortwave radiation forcing is the dashed lines and square points, and the incoming longwave radiation forcing is the dot-dashed lines and triangle points. [Colour figure can be viewed at wileyonlinelibrary.com]

the model, but it accounts for much more in the observations (up to 170% of the total daily LE). The shortwave radiation forcing term can also be affected by the diurnal variability of albedo, particularly in nonvegetated areas. In this study, we assume a constant albedo because we are focused on vegetated, irrigated areas where there is not a strong diurnal cycle of albedo.

The magnitude of the radiation—both the shortwave and the downwelling longwave components—forcing differs between the observations and the model across all scales, although these terms vary little between the scales. Although the model captures the magnitude of the radiation correctly, the radiation forcing term also includes a c_0 term which includes the rate of change of the saturation specific humidity as a function of temperature. This term is highly sensitive to small deviations in mixed-layer potential temperature, so small differences between the model and observation ABL temperature lead to large differences in the resulting c_0 term. Moreover, this term holds all of the errors between the model and observations, and it impacts the magnitude of every term in the LE tendency equation. Although this indicates that there are issues with direct comparison between the observations and the model, we can still evaluate the patterns from the observations. This error—along with other considerations when comparing results from the CLASS model and observational data directly—will be discussed further in Section 5.

Surface-layer feedbacks

The surface-layer feedback accounts for the turbulent transport of water vapour in the surface layer, where we assume constant fluxes and strong gradients. It generally reduces the LE over the course of the day at the regional and landscape scales, but it enhances LE at the local scale (Figure 7). This is because r_s remains near zero during the day because there is no water stress at the alfalfa local scale (see Appendix A). If we examine the diurnal cycle of the LE tendency due to the surface-layer feedback (see Appendix A for more information), we find its impacts are relatively small. The model shows that, for the regional and landscape scales, the surface-layer feedback is most negative in the morning and increases to near zero by the end of the day. At the local scale, the surface-layer feedbacks are positive over the course of the day, but they have a slight dip near midday. The observational terms have higher magnitude than the model term, but both the regional and landscape scales show the proper minimum value in this term at midday.

The match between model and observations is the worst for this term, most notably at the local and landscape scales. Because this term is controlled by r_a, it is sensitive to minor differences between the model and the observations. Moreover, we find that, although we can capture the magnitude of r_a for each scale, the trend between differs between model and observational r_a, leading to differences in the time derivative of r_a.

Land-surface feedbacks

The land-surface feedbacks contribute to the net reduction of LE during the day across all scales (Figure 5) through the surface temperature. The impact is strongest at the landscape scale. Figure 8 shows the separation of each term of the land-surface feedback: the G term, the L_{out} term (top panels), and the r_s term (bottom panels). The L_{out} and G

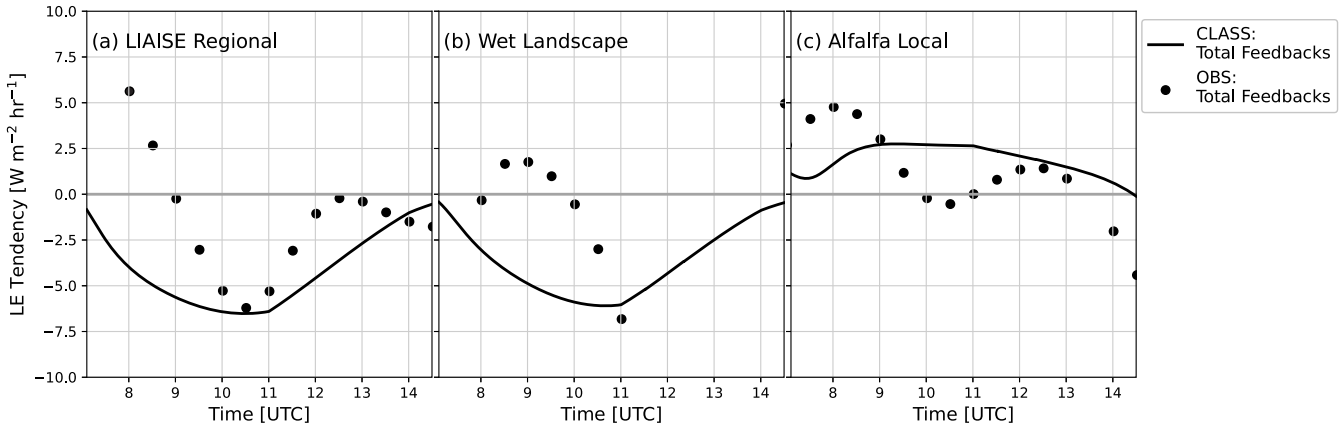

FIGURE 7 The surface-layer feedback for (a) the LIAISE regional scale, (b) the Wet Landscape scale, and (c) the Alfalfa Local scale. The observations are shown by the dots and the results from the CLASS model are shown by the lines.

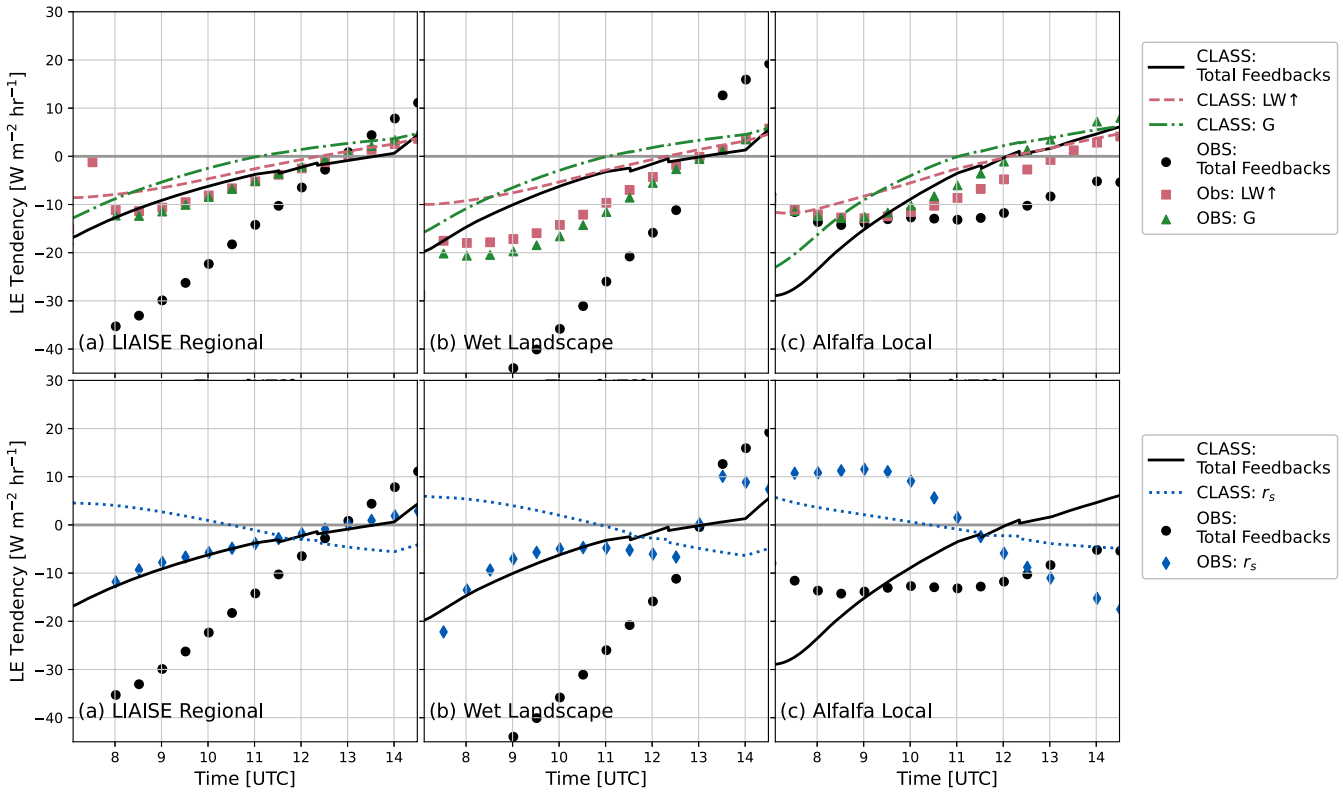

FIGURE 8 The diurnal cycles of the land-surface feedbacks are displayed for (a) the LIAISE regional scale, (b) the Wet Landscape scale, and (c) the Alfalfa Local scale. The observations are dots and the class model output is in lines. The top row has the outgoing longwave radiation and ground heat flux feedbacks, and the bottom row shows the surface resistance feedbacks. [Colour figure can be viewed at wileyonlinelibrary.com]

terms relate to the partitioning of available energy at the surface. Analogously, the r_s term represents the partitioning of available energy between LE and H at the surface. The land-surface feedback reduces LE until approximately 1300 UTC, then it enhances LE at the regional and landscape scales. Likewise, at the local scale, the land-surface feedbacks are negative in the morning and positive in the afternoon, but the change in tendency is not nearly linear like it is at larger spatial scales.

The G term follows the same pattern at all spatial scales. In the morning, this term reduces LE by removing net radiative energy, and in the afternoon energy that had previously been stored in the soil provides energy to enhance LE. L_{out} acts in the same manner: it reduces

LE during the morning and enhances it in the afternoon. At the regional and landscape scales, G reduces LE more than the L_{out} component, but during the afternoon they enhance LE comparably. At the local scale, the morning reduction from both G and L_{out} is smaller than at the landscape and regional scales. In the afternoon, the enhancement is stronger for the G component than the surface component. At the local scale, based on the land surface, there is more available energy to partition between H and LE than at larger scales.

The r_s component of the land-surface feedback follows a different pattern from the ground and longwave components because it does not exhibit as strong a diurnal cycle as the radiation-driven terms. Furthermore, there is a sign disagreement between the term from the CLASS model and that from observations. At the regional and landscape scales, the CLASS model shows that r_s enhances LE during the morning and that impact decreases over the course of the day, while observations show the opposite pattern. At the local scale, measurements and models agree that the r_s term increases LE during the morning and decreases it slightly after noon. At the local scale, the crops are well-watered and enhance LE; however, this process becomes more uncertain at larger spatial scales. This is because the difference in r_s between scales is driven by different soil-moisture regimes, and the observations for soil moisture become more uncertain at larger spatial scales. This disagreement between the models and the observations is due to the errors in the r_s term, which will be discussed in more detail in Section 5.

4.3 | Boundary-layer processes

The boundary-layer processes represent both the boundary-layer forcings and feedbacks. According to Figure 5, the boundary-layer forcings generally enhance LE, and they become particularly important at the local scale. This is case-dependent, as it is contingent on the prescribed advection. The boundary-layer feedbacks account for 20%–75% of the daily LE, and they are relatively more important at larger spatial scales. In this section, we examine both the boundary-layer forcing and feedback terms; however, we split the processes into local and nonlocal processes; see Figure 2. It is evident which processes are linked to the land surface and which are more related to interactions between the surfaces.

Local processes

The local boundary-layer processes—surface warming and moistening—impact the composition of the ABL and feedback on LE. The positive feedback of surface warming enhances LE over the course of the day; see Figure 9. This signal is closely coupled to that of the radiation and air temperature, as the peak enhancement of LE occurs near midday. It ranges from enhancing LE by $5\,W\,m^{-2}\,hr^{-1}$ in the morning and at the end of the afternoon to $10\,W\,m^{-2}\,hr^{-1}$ at noon at the regional scale. The impact of surface warming increases slightly at the landscape scale. At the local scale, there is more disagreement between the observations and model about the surface-warming feedback. The model shows the peak surface-warming impact above $5\,W\,m^{-2}\,hr^{-1}$, while the observations show an enhancement of LE much closer to zero, albeit still positive.

The surface-moistening feedback is a weak negative feedback across all scales; the magnitude of the reduction in LE is less than the enhancement from surface-heating feedback at larger spatial scales. From the observations, there is not a clear diurnal cycle in this feedback. The model output shows that the effect of surface LE is highest in the morning and decreases towards zero by the afternoon. The magnitude of this feedback is highest at the local scale. This indicates that at the local scale, where LE is higher and the ABL is shallower than at the regional scale, evaporation will eventually decrease due to the atmospheric conditions approaching saturation—without the influence of the nonlocal processes that are discussed in the next section.

Nonlocal processes

The nonlocal boundary-layer processes are the ones driven not only by the surface but also by larger-scale dynamics. Through these feedbacks, we can evaluate how patches of heterogeneity interact with each other to influence evaporation. The nonlocal processes cover the boundary-layer forcings (e.g., advection) and boundary-layer feedbacks (e.g. entrainment). Entrainment can enhance LE by both warming and drying the ABL (van Heerwaarden *et al.*, 2009).

In Figure 10, we show the results of the model and observations for the entrainment terms of the boundary-layer feedbacks. At the regional scale, the impact of entrainment warming and drying are both near zero, but they are positive over the day. At smaller scales, the impact of entrainment warming remains approximately the same, but the importance of entrainment drying becomes more important for enhancing LE at the local scale. The peak of entrainment effects is near midday for the regional scale, but moves to earlier in the day at the local scale because of the importance of entrainment drying. This could be because of the prescribed lapse rate

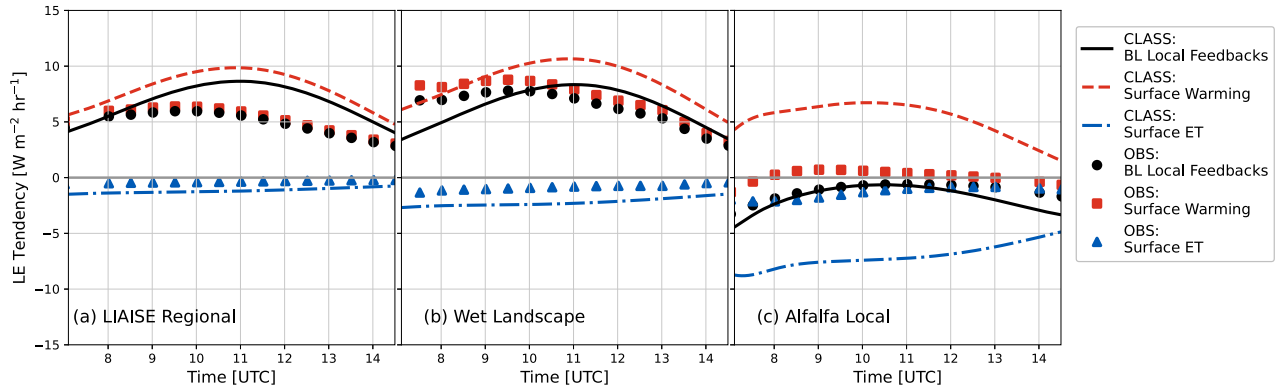

FIGURE 9 The terms of boundary-layer feedbacks of the local terms for (a) the LIAISE regional scale, (b) the wet landscape scale, and (c) the alfalfa local scale. Observations are points and results from the CLASS model are shown as lines. [Colour figure can be viewed at wileyonlinelibrary.com]

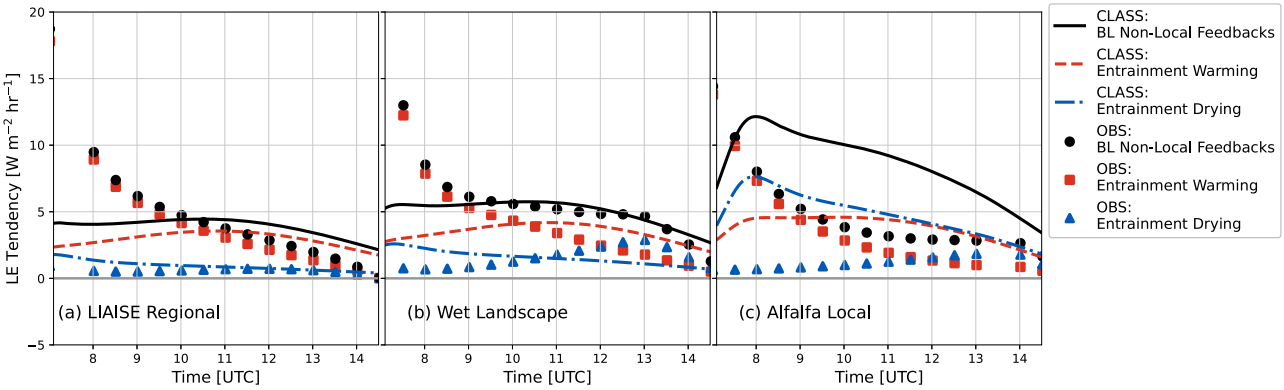

FIGURE 10 The terms of boundary-layer feedbacks of the nonlocal terms for (a) the LIAISE regional scale, (b) the wet landscape scale, and (c) the alfalfa local scale. Observations are points and results from the CLASS model are shown as lines. [Colour figure can be viewed at wileyonlinelibrary.com]

of the temperature in the free atmosphere. In the model, a daily average lapse rate is applied, while in reality a time-varying lapse rate might capture the entrainment response better, especially for warm-air entrainment. Radiosondes show that the potential temperature lapse rate decreases nearly linearly from 0.004 K m^{-1} in the morning to 0.001 K m^{-1} in the mid-afternoon. Furthermore, the observations show a peak enhancement of LE from entrainment in the mornings. The model and observations for entrainment drying disagree most at the local scale. The model indicates that entrainment drying becomes important, while observations again show its role is negligible.

In Figure 11, we display the results from the boundary-layer feedback terms for the regional, landscape, and local scales. Although the entrainment enhances evaporation and, in absolute value, is more important at the local scale, the boundary-layer forcing terms are equally important at the regional and landscape scales because the same advection of heat and moisture was prescribed. In the morning, the regional and landscape-scale advection is relatively low and constant, but at the end of the afternoon, when the sea breeze enters, advection of cool, moist air suppresses LE. Observations and the model match well for these scales. At the local scale, when stronger advection is prescribed, it enhances LE during the day. This is primarily through warm-air advection. The impact of moisture advection remains near zero throughout the entire day. The impact of dry-air advection is small compared with the impact of temperature advection across all spatial scales. This is explained in detail by vH10 and will be discussed in the subsequent section.

5 | DISCUSSION

We base our discussion on Figure 12, which shows the relative contribution of each term in the LE tendency equation to the daily LE for each spatial scale and between the

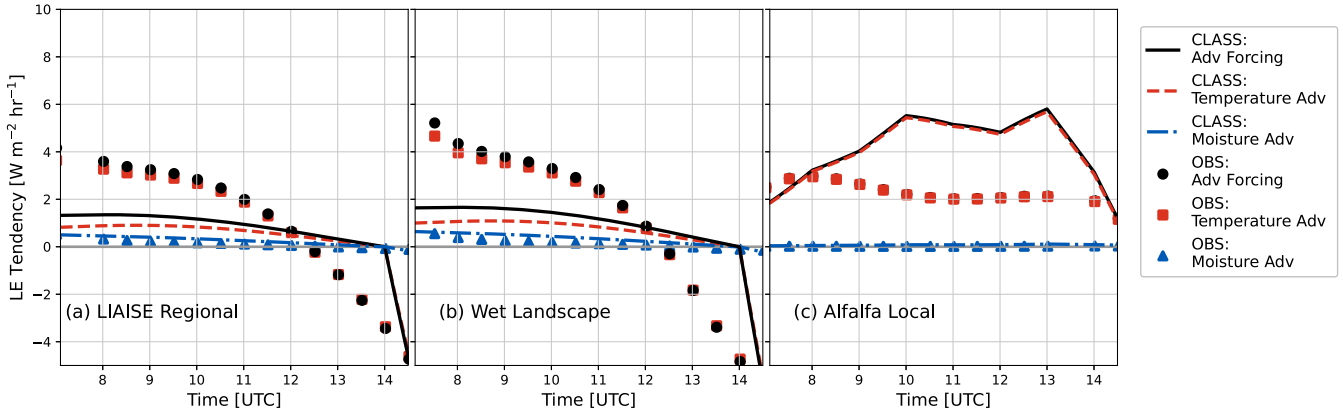

FIGURE 11 The terms of boundary-layer forcing of the nonlocal terms for (a) the LIAISE regional scale, (b) the wet landscape scale, and (c) the alfalfa local scale. Observations are points and results from the CLASS model are shown as lines. [Colour figure can be viewed at wileyonlinelibrary.com]

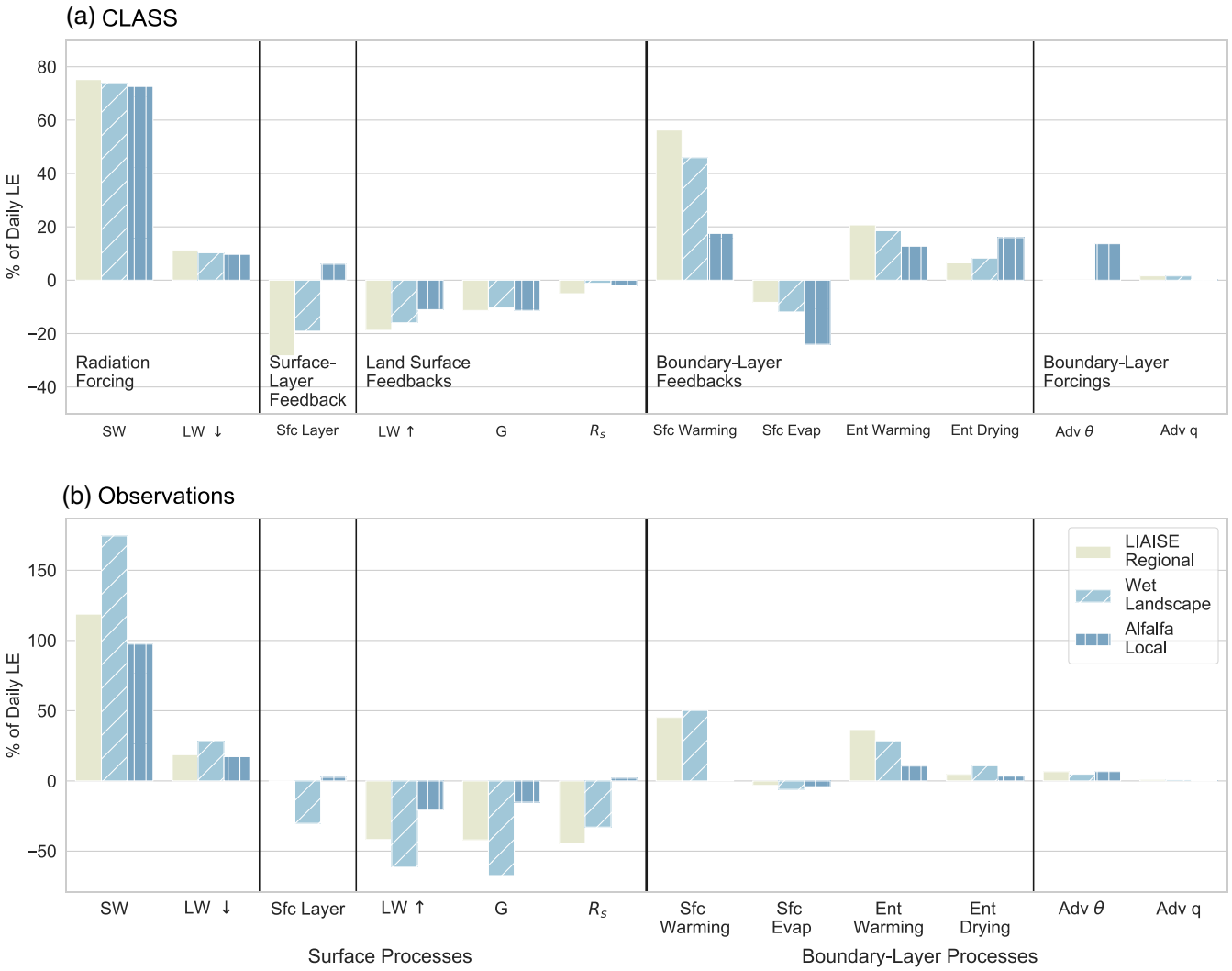

FIGURE 12 Terms in the latent heat tendency equation for the CLASS model experiments and the LIAISE observations weighted by their contribution to the total latent heat tendency from 0700–1700 UTC in the LIAISE domain. The spatial scale is indicated by hue and hatching, and each term is listed on the *x*-axis. The top panel is from the CLASS model and the bottom panel is from the observations. [Colour figure can be viewed at wileyonlinelibrary.com]

CLASS model (top) and the observations (bottom). We have chosen to show the relative contribution to daily LE instead of the absolute contribution to compare the impacts of scales directly. The absolute contributions show similar patterns, but the magnitudes are skewed due to the total LE at each scale. In Section 5.1, we compare individual processes across spatial scales by looking across the horizontal axis in Figure 12. It is important to note that, although the relative contribution for some processes (e.g., boundary-layer feedbacks) is higher at larger spatial scales, the absolute contribution of these processes to LE is lower than at the local scale. We focus the process-based discussion on the results of the LE tendency equation applied to output from the CLASS model, which integrates the scales to minimise errors based on the assumptions of mixed-layer theory. In this way, we apply the equation to a Penman–Monteith parameterisation of LE across three scales. In Section 5.2, we look across the vertical direction in Figure 12 to discuss briefly some of the differences between the model and observational results for the LE tendency equation. We argue that this method can be a valuable evaluation of the land-surface model representation. Additionally, we extrapolate the differences to discuss the implications for applying a mixed-layer model to heterogeneous areas.

5.1 | Integration across spatial scales

5.1.1 | Surface processes

In homogeneous land surfaces, we expect the surface and local boundary-layer processes to dominate the LE tendency. vH10 found comparable results for the radiation feedback with data from Cabauw and Niamey. In the LIAISE campaign, at the local scale, the plants were not water-stressed; however, at the regional scale, there were areas of nonirrigated crops which may have experienced water stress. The radiation feedbacks control the shape of the total LE tendency; however, the other terms, including boundary-layer processes, are significant in describing the timing of the LE. In this study, we find that the radiation feedbacks—mainly the incoming shortwave radiation—are responsible for the diurnal cycle in daily LE in this likely radiation-limited system, although we observe a phase lag of approximately 30 min between the peak radiation forcing and the peak LE across all spatial scales. From the CLASS model, we find that the relative impact of radiation increases at smaller spatial scales.

According to the LE tendency equation, the surface-layer feedbacks generally reduce LE at the regional and landscape scale and enhance it at the local scale. Both observations and the CLASS model indicate that this feedback contributes to enhancing LE at the local scale, although its cumulative daily effect is small from observations. On a diurnal cycle, we observe that this term can potentially strongly enhance or reduce LE, although its cumulative effect may be small. vH10 found a similar effect: the surface-layer feedbacks are near zero, except in the daytime transition periods. To reiterate the discussion from vH10, McNaughton and Spriggs (1986) found that LE is relatively insensitive to r_a. Our results suggest that this term may be important for enhancing or reducing LE under certain conditions, such as at the alfalfa local scale, where the surface is so evaporative that the surface layer is statically stable. This supports the finding from Lobos-Roco *et al.* (2021), who found that evaporation from a saline lake in the Atacama desert was controlled by wind. This term is also the most uncertain term based on observations, which is discussed in the next section.

We also find that the land surface reduces LE less in wetter locations (e.g., the alfalfa local scale) than it does in drier areas (e.g., the LIAISE regional scale). This corroborates the results from vH10, who found that at Cabauw the land-surface feedbacks reduce LE less than they do at Niamey. This is in part due to the land-surface cover and the way the energy is partitioned at the surface. Unlike the results from vH10, we find that, at the alfalfa local scale, the G and L_{out} feedbacks can enhance LE at the end of the day when the sea breeze arrives and cools and moistens the ABL. The land-surface enhancement of LE when the surface begins to provide energy for evaporation is partially responsible for the phase shift between LE and R_n.

The surface-driven processes account for a net enhancement of LE at the local scale from both models and observations; however, there is disagreement on the sign of the total contribution to LE between the model and observations and the regional and landscape scales. From the observations, there is a net enhancement of 13% (regional), 25% (landscape), and 83% (local) from all surface processes. Conversely, the CLASS model indicates that surface processes account for a 23% (regional), 34% (landscape), and 69% (local) enhancement of LE. Although there is disagreement on the magnitude, both the models and the observations indicate that the surface processes become relatively more important at smaller spatial scales.

5.1.2 | Boundary-layer processes

Boundary-layer processes are important for capturing the dynamic cycle of daily LE. The local processes are controlled directly from the land surface. We find that the local process of surface warming enhances LE more than surface moistening reduces it at larger scales. According

to the CLASS model, surface-driven boundary-layer processes enhance LE by 50% and 35% over the day at the regional and landscape scales, but reduce LE by 6% at the local scale. The reduction at the local scale is driven entirely by the surface-moistening feedback (Figure 9). The positive feedback at larger spatial scales is instead driven by the positive feedback of surface warming. We observe that the phase lag between radiation and LE is partially controlled by these local boundary-layer processes, mainly the surface-warming feedback (Figure 9). The impact of the surface-warming feedback peaks around noon, but it does not begin to reduce LE until the end of the afternoon.

We show that the nonlocal boundary-layer processes of entrainment warming and drying enhance LE across all scales for both observations and models. At the regional and landscape scales, we observe that the relative contribution of entrainment warming is constant between scales, but the impact of dry-air entrainment becomes more important at the local scale. Entrainment increases daily LE by approximately 20% according to the CLASS model (Figure 12). Entrainment enhances LE most in the morning, and it decreases to having little effect by the end of the afternoon (Figure 10). This indicates that in the morning, when the ABL is growing fastest, warm and dry air is entrained, enhancing LE. In the afternoon, when the ABL begins to grow more slowly (figure 8 of Mangan *et al.*, 2023), entrainment plays a less important role.

Advection is another important nonlocal process. At regional and landscape scales, we find that the impact of advection of heat and moisture on LE is relatively limited. In part, this can be explained by the prescribed synoptically driven advection at these scales. Likely there are errors in the magnitude of advection here, so it could play a more important role at these scales. At the local scale, where advection was calculated using data from an automated weather station network (Mangan *et al.*, 2023), advection enhances LE. We find that warm-air advection is responsible for enhancing LE more than dry-air advection. The reasons for this are twofold: (1) there is a nonlinear relationship between temperature and saturation vapour pressure, and in the temperature range of interest small increases in temperature increase the VPD more than small decreases of q (Clausius–Clapeyron Equation; figure 9 of vH10), and (2) the magnitude of the temperature advection is higher than that of the moisture advection. We have found that if we increase the magnitude of both moisture and temperature advection threefold, daily LE increases by approximately 10%. In our range of values, all of the increase in LE comes from stronger warm-air advection, and there is little influence from moisture advection. Further work should be done to verify whether these results are generalisable or site-specific.

5.1.3 | A note on the spatial scales selected

In this study, we have focused on the drivers of LE at progressively wetter spatial scales, from the LIAISE region to the irrigated landscape down to an individual alfalfa field. This is representative of an irrigation or "oasis effect" situation: a wet patch is within a larger drier regional scale. This is provided that the relevant length scales of surface and boundary-layer heterogeneity are selected in other situations. However, the opposite situation could occur: a dry patch is within a larger wetter regional scale. In the LIAISE domain, this situation can be approximated by evaluating the dry landscape and fallow local scales.

In the case of progressively drier scales, the dynamics of the atmospheric boundary layer are controlled more by the high sensible heat flux from the dry scale than in the case of the locally wet scale. Therefore, we expect different interactions between the scale of heterogeneity and the boundary-layer feedbacks on evapotranspiration with different surface Bowen ratios. For interested readers, we have included Appendix B, where we show the composite results for the LE tendency equation for the dry landscape scale. We find that the surface resistance feedback reduces LE where there is more water stress on the vegetation. We also find that, at the dry landscape scale, the surface and entrainment warming feedbacks become more important than at the wet landscape scales for enhancing LE.

5.2 | Latent heat tendency: Observations versus models

Although this study is focused primarily on the impacts of scale on the drivers of surface evaporation, we include both observational and model data. This warrants a brief discussion on the differences between the observational and model data, which is evident from the results shown in Section 4. This discussion is one part of a larger discussion the meteorological and land-surface modelling community should be having about how to integrate models with observations. We also make some recommendations for applying the mixed-layer framework to a heterogeneous environment.

As shown in Figures 5–12, there are notable differences between the magnitudes of the terms of the LE tendency equation between the CLASS model results and the observations. Generally, the models and observations agree on the signs of the terms, except notably in the surface and aerodynamic resistance feedback terms. We also observe that the LE tendency equation does not close when computed with observations, and its closure is worst at the local scale. There are some caveats for explaining the differences between the model results and observations and

explanations as to why any comparison between the two should be done with caution.

First, we imposed a number of assumptions on the observational data so that it mimics a mixed-layer model. We processed observational data so that it represents the associated variable in the CLASS model. For example, in order to upscale field-scale measurements to the landscape and regional scale, we create surface and flux maps using measurements from only the dominant crop covers. We also assume that radiosondes launched at local scales can represent all spatial scales above a blending height. Additionally, we calculated terms including r_a, r_s, and T_s with the same characterisations as the CLASS model, instead of relying on how they were observed directly. Finally, we imposed a polynomial fit to all of the data to remove some of its variability. These assumptions and forgoing physical observations for modelled data introduced some errors into the observational results, but they allowed us to make a homogeneous comparison of individual contributions to LE.

Second, we imposed a mixed-layer framework to observations that do not adhere to its assumptions. We observe an internal boundary layer in the wet area, but, by using a mixed-layer framework from the observed radiosondes, we assume there is no internal boundary layer at the local scale. This leads to inconsistencies between the observed and modelled boundary layer, particularly at the local scale. We find that the terms in the LE tendency equation do not sum up to the observed change in LE at any spatial scale, and we believe that this difference can be explained in part because of the failure of our assumptions.

Third, to interpret the results, we should consider c_0 that is multiplied by every term in the LE tendency equation (Equation 1). This term includes dq_{sat}/dT—the derivative of the saturation specific humidity with respect to temperature—which is highly sensitive to small changes in temperature, because of the aforementioned nonlinear relationship between temperature and saturation vapour pressure. Small deviations in temperature between the model and the observations yield changes in c_0, which are multiplied through each term in the equation. While any errors in this c_0 would not change the relative importance of a term (Figure 12), they can lead to large deviations in the magnitude of LE tendency terms. There is also the consideration of measurement height when comparing the model with observations. In this analysis, we selected our observations to match the model levels best. For example, we used mixed-layer values for temperature and humidity for c_0 (based on vertically integrated profiles observed using the soundings). Any agreement between the observational and model results is heavily dependent on the height of observation. This is particularly important for scalars within the surface layer and the ABL.

Finally, we find that if we calculate r_a using a mixed-layer value of wind and stability, we match the assumptions inherent in the LE tendency equation best, although we sacrifice true understanding of the surface conditions. We calculate a r_a that is a bulk, near-surface resistance term, where, in reality, instantaneous near-surface wind may control LE better. Near the surface, we observe stable stratification in the surface layer during the afternoon, while there is unstable stratification aloft. Because the CLASS model is unable to capture this complexity, we have selected mixed-layer wind for the r_a calculation from the radiosondes. We find that the LE tendency equation is sensitive to the formulation of the aerodynamic resistance—and therefore to the bulk surface resistance. Furthermore, we find that, although observations and the CLASS model agree on the magnitude of the r_a and r_s terms, they do not agree on the trend. This causes a sign disagreement in the surface-layer feedback term and the r_s component of the land-surface feedback term. The incorrect tendency in r_a appears to be due to the stability of the surface layer. We refer to Appendix A with additional figures to explain the r_a term.

Land-surface models in regional and global-scale weather models—including the one in the Integrated Forecasting System (IFS) from the European Centre for Medium-Range Weather Forecasts (ECMWF: (ECMWF, 2018; Hersbach *et al.*, 2020)) and the Noah-Multiparameterisation Land Surface Model (Noah-MP) in Weather Research and Forecasting (WRF: (Niu *et al.*, 2011))—employ the same assumptions as the CLASS model for partitioning the energy at the Earth's surface. Both models solve skin temperature by using a linearised surface-energy balance equation. By using the LE tendency approach, we can evaluate the performance of the model more thoroughly than by just comparing surface fluxes or atmospheric state variables. We can also apply the lessons learned using the CLASS model to understand better how LSMs handle surface heterogeneity. We find that the models have difficulty capturing stability in the surface layer, and that latent heat flux is sensitive to stability. Furthermore, this leads us to believe that global models will also have difficulty capturing the correct heat fluxes from locally stable conditions in an otherwise convective boundary layer. Improving land-surface representation, implementing high-resolution land-surface models, or implementing a mosaic approach for subgrid-scale heterogeneity where the tiles extend into the surface layer could improve this problem.

While there are several considerations to account for while comparing observations and numerical results—as in any study that attempts to verify a model with observations—these differences between observations and model results are large because we take a derivative of

the time series, which amplifies small differences. Generally, the LE tendency equation appears to give comparable results for observations and the CLASS model, which gives us confidence that the LE tendency equation is a reasonable diagnostic tool for understanding the drivers of evaporation, even if its mixed-layer assumptions do not hold.

6 | SUMMARY AND CONCLUSIONS

In this analysis, we use the LE tendency equation introduced by van Heerwaarden *et al.* (2010) to quantify the processes that drive the diurnal variability of evapotranspiration in a heterogeneous environment. Our main novel finding is that the scale of heterogeneity characterises the evapotranspiration limitation regimes: radiation-limited at the local scale and water-limited at the regional and landscape scales. We use a combination of observations and a coupled land–atmosphere model independently to replicate three scales of heterogeneity—regional, landscape, and local scale—based on the LIAISE field campaign of 2021. Using this framework, we characterise the processes that drive evapotranspiration as either surface processes (e.g., radiation forcing, land-surface feedback, and surface-layer feedback) or boundary-layer processes (e.g., boundary-layer forcings or feedbacks). We further distinguish local and nonlocal boundary-layer processes by identifying local (feedbacks from surface warming or moistening) and nonlocal (advection and entrainment of heat and moisture) drivers of LE.

By calculating the LE tendency equation independently from the mixed-layer model with observations from the LIAISE field campaign, we were able to evaluate the performance of the model outside its assumed mixed-layer framework. We found that the terms of the equation calculated from both the CLASS model and observations agree on the sign, although at times there are differences in the magnitude of the terms. The largest differences arise from the differences between how the aerodynamic and surface resistances are parameterised in the model and how these terms are parameterised based on observations. By using the framework of the LE tendency equation, we can verify the performance of LSMs at a parameter level, which can be a useful tool for improving the representation of surface fluxes over heterogeneous and complex terrain. Evaluating the land-surface scheme in these areas requires a spatial scale-driven approach.

In addition to evaluating the parameter-level performance of the CLASS model with the LE tendency equation, we focus on understanding how the processes that drive evapotranspiration change across spatial scales. In this study, we focus on three progressively wetter scales: regional, wet landscape, and alfalfa local scales. These scales are defined by the length scales of surface heterogeneity induced by irrigation and crop cover. Therefore, we address the following research questions using the results from the CLASS model.

1 *What are the processes that control evapotranspiration across spatial scales in a heterogeneous environment?*

The surface-driven properties enhance daily evapotranspiration at all scales, but they become relatively more important at the smaller spatial scales. Over the course of the day, surface-driven processes enhance LE between 23% at the regional scale and 64% at the local scale. Radiation forcing is relatively most important at the landscape scale, with a daily LE enhancement of 87%. The land-surface feedbacks reduce LE at all scales by between 25% and 30%. The G feedback decreases LE most at the local scale ($\sim$ 10% reduction in daily LE). Surface resistance reduces LE least when the surface is wettest at smaller spatial scales, which suggests that evapotranspiration is not limited by water at the local scale. We find that the energy stored in the surface supplies energy to boost evapotranspiration at the local scale during the afternoon, which might explain the phase shift between R_n and LE observed at the local scale (Figure 3).

Like the surface processes, the boundary-layer processes enhance LE at all scales, but their impact is highest at the regional and landscape scales (77% and 64% enhancement of daily LE) and becomes less important at the local scale (36% of daily LE). This pattern is mainly driven by the surface-warming feedback. At the regional scale, where the land surface is relatively warm and dry, sensible heating is relatively high, which heats the ABL, enhancing LE. This feedback can also explain the phase shift between LE and R_n. At the local scale, the surface-moistening feedback reduces LE. The surface is wet and highly evaporative, which causes the ABL to approach saturation, reducing LE. Finally, warm-air advection has an important role in enhancing LE at the local scale, while dry-air advection has a relatively small impact on the magnitude of LE.

2 *What is the relative importance of nonlocal (i.e., advection and entrainment) controls on surface fluxes in an idealised heterogeneous area?*

Nonlocal controls, including advection and entrainment of heat and moisture, play an important role in enhancing LE at the local scale. Nonlocal processes contribute 27% of the daily LE at the regional scale, increasing to 43% at the local scale. This effect is due mainly to the entrainment of warm air, which is equally important for enhancing LE at all scales. At the local scale, the drying process from entrainment becomes more important, because it introduces much drier air than the existing mixed layer. Like

entrainment, advection is an important term in controlling evapotranspiration at the local level and becomes less important at larger spatial scales. At the local scale, the advection of warm air accounts for 14% of the total daily LE, while the advection of dry air nominally increases daily LE (~3%). This effect is because a small increase in temperature accounts for a large increase in the vapour-pressure deficit in the temperature range examined in this case.

3 *How do the contributions of evapotranspiration blend across spatial scales?*

At the local scale, the surface properties and nonlocal boundary-layer processes like advection and entrainment control evapotranspiration, while at the regional and landscape scales local boundary-layer processes like feedbacks with the boundary-layer become important for controlling evapotranspiration. Although in our framework scales of heterogeneity are noninteracting, in reality the regional and landscape scales are built from integrating processes that occur at local scales. This implies that on an individual field scale the land surface controls land–atmosphere interactions, but at larger scales the properties of the ABL begin to determine surface fluxes. This has implications for the land-surface modelling community, as the type of model error could depend on the scale of the process.

The LE tendency equation allows us to determine the drivers of evapotranspiration at all spatial scales by assuming mixed-layer theory. It can also be applied to the output of various weather and climate models that employ the Penman–Monteith formulation of LE to diagnose the processes that drive LE. We find that, in relative terms, the local boundary-layer processes (surface warming and moistening) enhance LE at larger spatial scales. At the local scale, nonlocal ABL effects (entrainment and advection) enhance LE. We find that, although the model and observations agree reasonably well with surface fluxes and atmospheric state variables, parameterised resistance terms have a poor match between models and observations. Further work should be done to understand the impact of these terms in capturing surface dynamics in a heterogeneous environment.

AUTHOR CONTRIBUTIONS

Mary Rose Mangan: conceptualization; formal analysis; investigation; writing – original draft. **Oscar Hartogensis:** conceptualization; supervision; writing – review and editing. **Chiel van Heerwaarden:** conceptualization; methodology; writing – review and editing. **Jordi Vilà-Guerau de Arellano:** conceptualization; supervision; writing – review and editing.

ACKNOWLEDGEMENTS

We thank the hosts, organisers, and participants of the LIAISE campaign. This PhD project was partly supported by the appointment of Jordi Vila as Chair of the Meteorology and Air Quality Group of Wageningen University.

CONFLICT OF INTEREST STATEMENT

The authors have no conflicts of interest to declare.

DATA AVAILABILITY STATEMENT

Data collected during the LIAISE campaign are archived at https://liaise.aeris-data.fr/. Due to the nature of the experiment, data are not yet available for public download. Data can be provided directly from the authors upon request.

ORCID

Mary Rose Mangan https://orcid.org/0000-0002-9017-7939

REFERENCES

Abdel-Aziz, M.H., Taylor, S.A. and Ashcroft, G.L. (1964) Influence of advective energy on transpiration. *Agronomy Journal*, 56, 139–142 https://onlinelibrary.wiley.com/doi/pdf/10.2134/agronj1964.00021962005600020005x.

Ball, F.K. (1960) Control of inversion height by surface heating. *Quarterly Journal of the Royal Meteorological Society*, 86, 483–494.

Boone, A., Bellvert, J., Best, M., Brooke, J., Canut-Rocafort, G., Cuxart, J., Hartogensis, O., Moigne, P., Miró, J.R., Polcher, J., Price, J., Quintana Segu, P. and Wooster, M. (2021) Updates on the international land surface interactions with the Atmophere over the Iberian semi-arid environment (LIAISE) field campaign. *GEWEX News*, 31, 17–21.

Butterworth, B.J., Desai, A.R., Townsend, P.A., Petty, G.W., Andresen, C.G., Bertram, T.H., Kruger, E.L., Mineau, J.K., Olson, E.R., Paleri, S., Pertzborn, R.A., Pettersen, C., Stoy, P.C., Thom, J.E., Vermeuel, M.P., Wagner, T.J., Wright, D.B., Zheng, T., Metzger, S., Schwartz, M.D., Iglinski, T.J., Mauder, M., Speidel, J., Vogelmann, H., Wanner, L., Augustine, T.J., Brown, W.O.J., Oncley, S.P., Buban, M., Lee, T.R., Cleary, P., Durden, D.J., Florian, C.R., Lantz, K., Riihimaki, L.D., Sedlar, J., Meyers, T.P., Plummer, D.M., Guzman, E.R., Smith, E.N., Sühring, M., Turner, D.D., Wang, Z., White, L.D. and Wilczak, J.M. (2021) Connecting land–atmosphere interactions to surface heterogeneity in CHEESEHEAD19. *Bulletin of the American Meteorological Society*, 102, E421–E445.

Cuxart, J. and Boone, A.A. (2020) Evapotranspiration over land from a boundary-layer meteorology perspective. *Boundary-Layer Meteorology*, 177, 427–459.

Cuxart, J., Wrenger, B., Mart, D., Reuder, J., Jonassen, M.O., Jiménez, M.A., Lothon, M., Lohou, F., Hartogensis, O., Dünnermann, J., Conangla, L. and Garai, A. (2016) Estimation of the advection effects induced by surface heterogeneities in the surface energy budget. *Atmospheric Chemistry and Physics*, 16, 9489–9504.

Driedonks, A.G.M. and Tennekes, H. (1984) Entrainment effects in the well-mixed atmospheric boundary layer. *Boundary-Layer Meteorology*, 30, 75–105.

ECMWF. (2018) *IFS Documentation CY45R1-Part IV: Physical Processes*. Reading, UK: IFS Documentation.

Ek, M.B. and Holtslag, A. (2004) Influence of soil moisture on boundary layer cloud development. *Journal of Hydrometeorology*, 5, 86–99.

Hersbach, H., Bell, B., Berrisford, P., Hirahara, S., Horányi, A., Muñoz-Sabater, J., Nicolas, J., Peubey, C., Radu, R., Schepers, D., Simmons, A., Soci, C., Abdalla, S., Abellan, X., Balsamo, G., Bechtold, P., Biavati, G., Bidlot, J., Bonavita, M., De Chiara, G., Dahlgren, P., Dee, D., Diamantakis, M., Dragani, R., Flemming, J., Forbes, R., Fuentes, M., Geer, A., Haimberger, L., Healy, S., Hogan, R.J., Hólm, E., Janisková, M., Keeley, S., Laloyaux, P., Lopez, P., Lupu, C., Radnoti, G., de Rosnay, P., Rozum, I., Vamborg, F., Villaume, S. and Thépaut, J.-N. (2020) The ERA5 global reanalysis. *Quarterly Journal of the Royal Meteorological Society*, 146, 1999–2049 https://onlinelibrary.wiley.com/doi/pdf/10.1002/qj.3803.

Higgins, C.W., Pardyjak, E., Froidevaux, M., Simeonov, V. and Parlange, M.B. (2013) Measured and estimated water vapor advection in the atmospheric surface layer. *Journal of Hydrometeorology*, 14, 1966–1972.

Inagaki, A., Letzel, M.O., Raasch, S. and Kanda, M. (2006) Impact of surface heterogeneity on energy imbalance: a study using LES. *Journal of the Meteorological Society of Japan. Series II*, 84, 187–198.

Jacobs, A.F.G., van Boxel, J.H. and Shaw, R.H. (1992) The dependence of canopy layer turbulence on within-canopy thermal stratification. *Agricultural and Forest Meteorology*, 58, 247–256.

Jacobs, C.M.J. and Bruin, H.A.R. (1992) The sensitivity of regional transpiration to land-surface characteristics: significance of feedback. *Journal of Climate*, 5, 683–698.

Jarvis, P.G., Monteith, J.L. and Weatherley, P.E. (1976) The interpretation of the variations in leaf water potential and stomatal conductance found in canopies in the field. *Philosophical Transactions of the Royal Society of London. B, Biological Sciences*, 273, 593–610.

Kanda, M., Inagaki, A., Letzel, M.O., Raasch, S. and Watanabe, T. (2004) LES study of the energy imbalance problem with Eddy covariance fluxes. *Boundary-Layer Meteorology*, 110, 381–404.

Lobos-Roco, F., Hartogensis, O., Vilà-Guerau de Arellano, J., de la Fuente, A., Muñoz, R., Rutllant, J. and Suárez, F. (2021) Local evaporation controlled by regional atmospheric circulation in the Altiplano of the Atacama Desert. *Atmospheric Chemistry and Physics*, 21, 9125–9150.

Mangan, M.R., Hartogensis, O., Boone, A., Branch, O., Canut, G., Cuxart, J., de Boer, H.J., Le Page, M., Mart, D., Miró, J.R., Price, J. and Vilà-Guerau de Arellano, J. (2023) The surface-boundary layer connection across spatial scales of irrigation-driven thermal heterogeneity: an integrated data and modeling study of the LIAISE field campaign. *Agricultural and Forest Meteorology*, 335, 109452.

McNaughton, K.G. and Spriggs, T.W. (1986) A mixed-layer model for regional evaporation. *Boundary-Layer Meteorology*, 34, 243–262.

Niu, G.-Y., Yang, Z.-L., Mitchell, K.E., Chen, F., Ek, M.B., Barlage, M., Kumar, A., Manning, K., Niyogi, D., Rosero, E., Tewari, M. and Xia, Y. (2011) The community Noah land surface model with multiparameterization options (Noah-MP): 1. Model description and evaluation with local-scale measurements. *Journal of Geophysical Research: Atmospheres*, 116, D12109.

Noilhan, J. and Mahfouf, J.F. (1996) The ISBA land surface parameterisation scheme. *Global and Planetary Change*, 13, 145–159.

Noilhan, J. and Planton, S. (1989) A Simple parameterization of land surface processes for meteorological models. *Monthly Weather Review*, 117, 536–549.

Patton, E.G., Sullivan, P.P. and Moeng, C.-H. (2005) The influence of idealized heterogeneity on wet and dry planetary boundary layers coupled to the land surface. *Journal of the Atmospheric Sciences*, 62, 2078–2097.

Raupach, M.R. (2000) Equilibrium evaporation and the convective boundary layer. *Boundary-Layer Meteorology*, 96, 107–142.

Renner, M., Kleidon, A., Clark, M., Nijssen, B., Heidkamp, M., Best, M. and Abramowitz, G. (2021) How well can land-surface models represent the diurnal cycle of turbulent heat fluxes? *Journal of Hydrometeorology*, 22, 77–94.

Rosenberg, N.J. (1969) Seasonal patterns in evapotranspiration by irrigated alfalfa in the central great plains1. *Agronomy Journal*, 61, 879–886 https://onlinelibrary.wiley.com/doi/pdf/10.2134/agronj1969.00021962006100060015x.

Steinfeld, G., Letzel, M.O., Raasch, S., Kanda, M. and Inagaki, A. (2007) Spatial representativeness of single tower measurements and the imbalance problem with eddy-covariance fluxes: results of a large-eddy simulation study. *Boundary-Layer Meteorology*, 123, 77–98.

Stewart, J.B. (1988) Modelling surface conductance of pine forest. *Agricultural and Forest Meteorology*, 43, 19–35.

Stoy, P.C., Mauder, M., Foken, T., Marcolla, B., Boegh, E., Ibrom, A., Arain, M.A., Arneth, A., Aurela, M., Bernhofer, C., Cescatti, A., Dellwik, E., Duce, P., Gianelle, D., van Gorsel, E., Kiely, G., Knohl, A., Margolis, H., McCaughey, H., Merbold, L., Montagnani, L., Papale, D., Reichstein, M., Saunders, M., Serrano-Ortiz, P., Sottocornola, M., Spano, D., Vaccari, F. and Varlagin, A. (2013) A data-driven analysis of energy balance closure across FLUXNET research sites: the role of landscape scale heterogeneity. *Agricultural and Forest Meteorology*, 171-172, 137–152.

Stull, R.B. (1988) *An Introduction of Boundary Layer Meteorology*. Dordrecht: Kluwer.

Tennekes, H. (1973) A model for the dynamics of the inversion above a convective boundary layer. *Journal of the Atmospheric Sciences*, 30, 558–567.

Twine, T.E., Kustas, W.P., Norman, J.M., Cook, D.R., Houser, P.R., Meyers, T.P., Prueger, J.H., Starks, P.J. and Wesely, M.L. (2000) Correcting eddy-covariance flux underestimates over a grassland. *Agricultural and Forest Meteorology*, 103, 279–300.

van Heerwaarden, C.C., Mellado, J.P. and Lozar, A.D. (2014) Scaling Laws for the heterogeneously heated free convective boundary layer. *Journal of Atmospheric Sciences*, 71, 3975–4000.

van Heerwaarden, C.C., Vilà-Guerau de Arellano, J., Gounou, A., Guichard, F. and Couvreux, F. (2010) Understanding the daily cycle of evapotranspiration: a method to quantify the influence of Forcings and feedbacks. *Journal of Hydrometeorology*, 11, 1405–1422.

van Heerwaarden, C.C., Vilà-Guerau de Arellano, J., Moene, A.F. and Holtslag, A.A.M. (2009) Interactions between dry-air entrainment, surface evaporation and convective boundary-layer development. *Quarterly Journal of the Royal Meteorological Society*, 135, 1277–1291.

Vilà-Guerau de Arellano, J., van Heerwaarden, C.C., van Stratum, B.J.H. and van den Dries, K. (2015) *Atmospheric Boundary Layer:*

Integrating Chemistry and Land Interactions. New York, New York: Cambridge University Press.

Wilson, M.F., Henderson-Sellers, A., Dickinson, R.E. and Kennedy, P.J. (1987) Sensitivity of the biosphere–atmosphere transfer scheme (BATS) to the inclusion of variable soil characteristics. *Journal of Applied Meteorology and Climatology*, 26, 341–362.

How to cite this article: Mangan, M.R., Hartogensis, O., van Heerwaarden, C. & Vilà-Guerau de Arellano, J. (2023) Evapotranspiration controls across spatial scales of heterogeneity. *Quarterly Journal of the Royal Meteorological Society*, 149(756), 2696–2718. Available from: https://doi.org/10.1002/qj.4527

APPENDIX A. FORMULATION OF RESISTANCE TERMS

In order to use the LE tendency equation (Equation 1) for experimental data, we calculated the resistance terms (both surface and aerodynamic) using parameterisations from the CLASS model's land-surface scheme. In this way, we were able to calculate dynamically changing resistance terms, which were necessary for computing the LE tendency equation.

The aerodynamic resistance, which is an important term in the surface-layer feedback term, is computed using the Businger–Dyer surface-layer relationship for the surface layer (Stull, 1988). The aerodynamic resistance (r_a) is a function of a drag coefficient (C_s) and the effective wind speed (U_{eff}). The r_a term is shown in Figure A1a–c:

$$r_a = (C_s\, U_{eff}\,)^{-1}, \tag{A1}$$

where the drag coefficient,

$$C_s = \frac{\kappa^2}{\left[\ln\left(\frac{z_{sl}}{z_{0h}}\right) - \Psi_h\left(\frac{z_{sl}}{L}\right) + \Psi_h\left(\frac{z_{0h}}{L}\right)\right]\left[\ln\left(\frac{z_{sl}}{z_{0m}}\right) - \Psi_m\left(\frac{z_{sl}}{L}\right) + \Psi_m\left(\frac{z_{0m}}{L}\right)\right]}, \tag{A2}$$

is a function of the von Kármán constant ($\kappa = 0.4$), the Obukhov length (L), the Businger–Dyer relations for

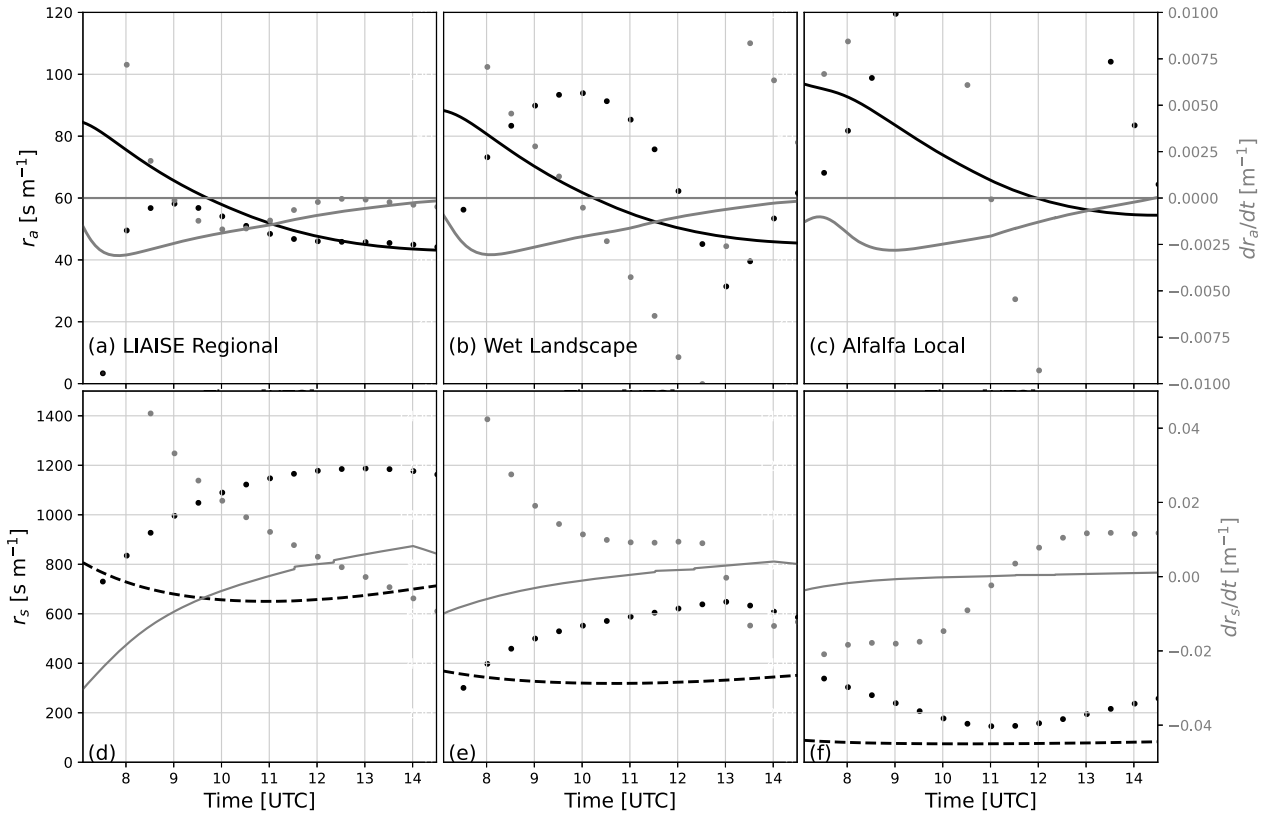

FIGURE A1 (a–c) The r_a component for the CLASS model (lines) and observations (dots) for (a) the LIAISE regional, (b) wet landscape, and (c) alfalfa local scales. (d–f) The $r_{s_{bulk}}$ component for the CLASS model (lines) and observations (dots) for (d) the LIAISE regional, (e) wet landscape, and (f) alfalfa local scales. In all panels, the black dots and lines are the values of r_a and $r_{s_{bulk}}$, and the grey are the derivatives of each term.

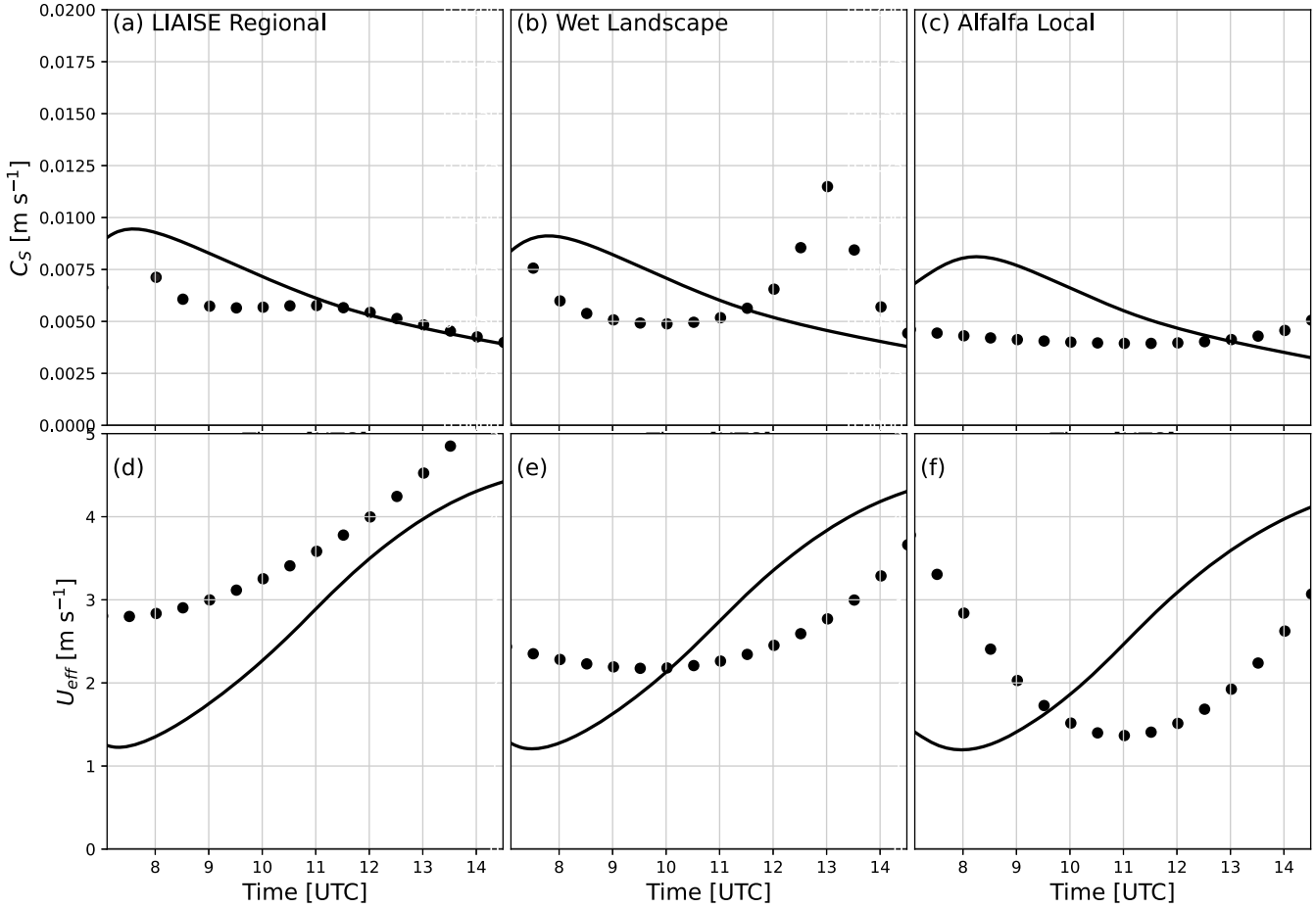

FIGURE A2 (a–c) The stability-based component of r_a for the CLASS model (lines) and observations (dots) for (a) the LIAISE regional, (b) wet landscape, and (c) alfalfa local scales. (d–f) The wind-driven component of r_a for the CLASS model (lines) and observations (dots) for (d) the LIAISE regional, (e) wet landscape, and (f) alfalfa local scales.

momentum and heat transport (Ψ_m, Ψ_h), the height of the surface layer (z_{sl}), and the roughness length for momentum and heat (z_{0m}, z_{0h}). The effective wind speed,

$$U_{\text{eff}} = \sqrt{(U^2 + w_*^2)}, \tag{A3}$$

is a function of the mean wind speed (U) and the convective velocity scale (w_*) for the mixed layer. The U_{eff} and C_s terms are shown in Figure A2.

Finally, we compute a bulk r_s based on the aerodynamic resistance:

$$r_{s_{\text{bulk}}} = \rho \frac{L_v}{LE}\left(\frac{dq_{\text{sat}}}{dT}(T_s - \theta) + (q_{\text{sat}} - q)\right) - r_a, \tag{A4}$$

where the variables used in the equation have been defined in Section 3, and T_s and q are mixed-layer variables. The surface resistance is shown in panels Figure A1d–f.

APPENDIX B. LE TENDENCY IN THE DRY LANDSCAPE SCALE

The wet landscape scale of the LIAISE region consists mainly of nonirrigated agricultural fields of vineyards, orchards, and harvested cereal crops. We have computed the LE tendency equation at the dry landscape scale, where the observed daily LE peaks around 100 W m^{-2}. We have not included the fallow local scale in this analysis, because the observed daily LE peaks around 10 W m^{-2}.

Figure B1 shows the relative contribution of each term in the LE tendency equation to the daily LE for each spatial scale and between the CLASS model (top) and the observations (bottom), like Figure 12 including the dry landscape scale. The radiation terms are comparable to those in the irrigated area. The surface-layer feedbacks reduce LE more at the dry landscape scale than in the wet landscape scale. Likewise, with the land-surface feedbacks, we find that energy partitioning into the surface reduces LE more than at wetter scales. Furthermore, the

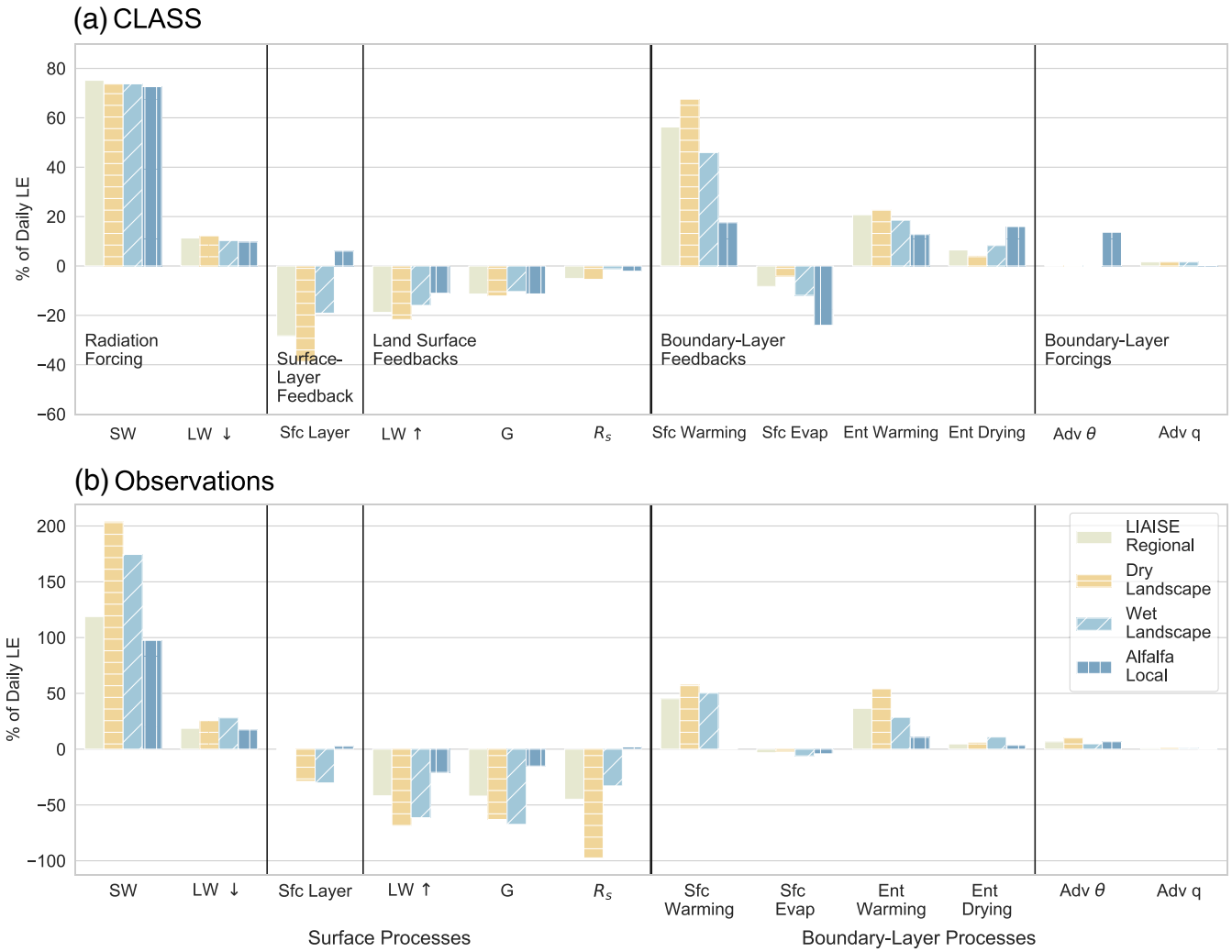

FIGURE B1 Terms in the latent heat tendency equation for the CLASS model experiments and the LIAISE observations weighted by their contribution to the total latent heat tendency from 0700–1700 UTC in the LIAISE domain for the LIAISE regional, wet, and dry landscape scales and alfalfa local scales. The spatial scale is indicated by hue and hatching, and each term is listed on the *x*-axis. The top panel is from the CLASS model and the bottom panel is from the observations. [Colour figure can be viewed at wileyonlinelibrary.com]

surface resistance feedback becomes more important. This is related to the water stress that arises because the dry landscape scale moves into a water-limited regime. Lastly, the boundary-layer feedbacks show an important difference from the wet scales. The surface and entrainment feedbacks enhance LE relatively more than at the wetter spatial scales. This is because the boundary layer is warmer at this scale because of the high sensible heat flux. The surface evaporation feedback reduces LE less at this scale as well compared with wetter scales.

At the diurnal scale, the pattern of the dry landscape scale resembles that of the regional scale, except that the magnitudes are lower because of the lower magnitude of the total LE. This indicates that the sensible heat flux from the dry landscape dominates the atmospheric boundary layer observed at the regional scale. For this reason, we do not show the results of the diurnal cycles for the dry landscape scale.